Deglacial temperature and carbonate saturation state variability in the tropical Atlantic at Antarctic Intermediate Water Depths

D. W. Oppo[1, *], W. Lu[1], K.-F. Huang[2], N. E. Umling[3], W. Guo[1], J. Yu[4,5], W. B. Curry[6], T. M. Marchitto[7], S. Wang[1,8]

[1]Woods Hole Oceanographic Institution, Woods Hole, Massachusetts, USA.

[2]Institute of Earth Sciences, Academia Sinica, Taipei, Taiwan.

[3]Rutgers University, New Brunswick, New Jersey

[4]Laoshan Laboratory, Qingdao, China

[5]Research School for Earth Sciences, The Australian National University, Canberra, Australian Capital Territory, Australia

[6]Bermuda Institute of Ocean Sciences, St. George's, Bermuda.

[7]Department of Geological Sciences and Institute of Arctic and Alpine Research, University of Colorado, Boulder, Colorado, USA.

[8] MIT-WHOI Joint Program in Oceanography/Applied Ocean Sciences & Engineering, Cambridge and Woods Hole, MA, USA

Corresponding Author: Delia W. Oppo (doppo@whoi.edu)

Key Points

- Regional warming occurred in the tropical Atlantic at Antarctic Intermediate Water depths during Heinrich Stadial 1
- Deglacial nutrient and $\Delta[CO_3^{2-}]$ trends and variability suggest a strong link between AMOC intensity and AAIW northward extent
- Deglacial $\Delta[CO_3^{2-}]$ trends and variability likely affected upper Atlantic temperature estimates based on Mg/Ca of foraminifera

Abstract

Variations in the Atlantic Meridional Overturning Circulation (AMOC) redistribute heat and nutrients, causing pronounced anomalies of temperature and nutrient concentrations in the subsurface ocean. However, exactly how millennial-scale deglacial AMOC variability influenced the subsurface is debated, and the role of other deglacial forcings of subsurface temperature change is unclear. Here, we present a new deglacial temperature reconstruction, which, with published records, helps assess competing hypotheses for deglacial warming in the upper tropical North Atlantic. Our record provides new evidence of regional subsurface warming in the western tropical North Atlantic within the core of modern Antarctic Intermediate Water (AAIW) during Heinrich Stadial 1 (HS1), an early deglacial interval of iceberg discharge into the North Atlantic. Our results are consistent with model simulations that suggest subsurface heat accumulates in the northern high-latitude convection regions and along the upper AMOC return path when the AMOC weakens, and with warming due to rising greenhouse gases. Warming of AAIW may have also contributed to warming in the tropics at modern AAIW depths during late HS1. Nutrient and $\Delta[CO_3^{2-}]$ reconstructions from the same site suggest a link between AMOC intensity and the northward extent of AAIW in the northern tropics across the deglaciation and on millennial time scales. However, the timing of the initial deglacial increase in AAIW to the northern tropics is ambiguous. Deglacial trends and variability of $\Delta[CO_3^{2-}]$ in the upper North Atlantic have likely biased temperature reconstructions based on the elemental composition of calcitic benthic foraminifera.

Plain Language Summary

The Atlantic Meridional Overturning Circulation (AMOC) is characterized by northward flow in the upper ocean and southward flow in the deep ocean. Understanding how the AMOC has changed in the past, and how such changes have affected surface climate and the distribution of ocean heat, carbon, and nutrients is important but challenging, as reconstructions of subsurface ocean properties are sometimes ambiguous. Here, we use the chemical composition of seafloor shells from a site in the western tropical Atlantic Ocean at ~ 950 meters water depth, within the northward-flowing limb of the AMOC, to reconstruct temperature, nutrients, and carbon content during the end of the last Ice Age, an interval when AMOC strength is believed to have varied. Our results support a link between AMOC strength and tropical Atlantic nutrient content, and

further suggest that both rising atmospheric CO_2 and AMOC variations influenced temperatures and carbon in the subsurface tropical Atlantic Ocean.

1 Introduction

During the last deglaciation, disintegration of continental ice sheets added freshwater to the ocean (e. g. Bond et al., 1993), atmospheric CO_2 rose (e.g., Barnola et al., 1987), and the Atlantic Meridional Overturning Circulation (AMOC) seems to have varied in strength (e.g., McManus et al., 1994; Rafter et al., 2022). Reconstructions suggest the AMOC was weaker during North Atlantic millennial-scale cold events – Heinrich Stadial 1 (HS1; ~ 18 to 14.7 thousand years ago, ka) and the Younger Dryas (YD; 12.9 to 11 ka) – compared to the Last Glacial Maximum (LGM, ~ 23 to 19 ka), the Bølling-Allerød (BA; ~14.7 to 12.9 ka), and the Holocene (e.g., McManus et al., 1994; Ng et al., 2018).

Deglacial AMOC variability has been proposed to alter the subsurface ocean's temperature and nutrient distributions but the driving mechanisms are still uncertain. Many model simulations suggest that in response to a reduced AMOC, heat initially accumulates above ~ 2 km in the subpolar North Atlantic convection regions (e. g. Liu et al., 2009; Zhang et al., 2017). Early deglacial upper-ocean warming may have promoted basal melting of ice sheets (Marcott et al., 2011) and helped maintain high surface buoyancy, sustaining a weak AMOC through HS1 (Ng et al., 2018). Model simulations suggest that the upper North Atlantic warming propagates southward along the Deep Western Boundary Current into the South Atlantic, and eventually into the Indian and Pacific Oceans (Pedro et al., 2018). In models, the South Atlantic and tropical thermoclines warm during events of AMOC weakening due to the reduced northward transport of warm upper ocean waters required to replace the southward export of deep waters formed in the North Atlantic (e. g. Dahl et al., 2005; Pedro et al., 2018; Zhang et al., 2007).

However, in a transient experiment of the last 21,000 years (TraCE-21K) (Liu et al., 2009), much of the shallow (< 1000 m) North Atlantic cools, not warms, during the simulated YD even though the AMOC weakens, contrasting with the warming response during the simulated HS1 (He et al., 2020; Umling et al., 2019). Additional freshwater simulations suggest that the subsurface response to reduced AMOC reflects a competition between reduced deep convection in the North Atlantic, a change which warms the subsurface North Atlantic, and reduced northward (cross-equatorial) heat advection, which cools the subsurface North Atlantic (He et al., 2020). In these experiments, when a surface freshening threshold is crossed, the subsurface response changes from cooling to warming. In TraCE-21K, reduced deep convection dominates the simulated HS1 (warming) response due to the strong and prolonged freshwater forcing and AMOC response, whereas reduced northward heat advection dominates the simulated YD (cooling), when the simulated freshwater forcing and AMOC response are weaker. In both cases, reduced northward heat transport results in warming of the South Atlantic and tropical thermoclines. Although the details of the anomalous temperature distribution response to surface freshwater-induced AMOC weakening likely differ among models, in the TraCE-21K freshwater forcing simulation, the boundary between shallow (< 1000 m) southern warming and northern cooling is north of the equator during the YD (He et al., 2020).

In TraCE-21K (Liu et al., 2009), decreasing the elevation of the Laurentide ice sheet also causes an AMOC decrease (Zhu et al., 2014), warming in the upper 2000 m, especially in the North Atlantic (Umling et al., 2019). Model simulations suggest that rising greenhouse gases also warmed the subsurface (e. g., Liu et al., 2009; Menviel et al., 2015; Umling et al., 2019). Finally, some investigators suggest that Southern Ocean warming during North Atlantic cold events was transmitted northward within Antarctic Intermediate Water (AAIW), warming the tropical North Atlantic (Hines et al., 2019; Poggemann et al., 2017, 2018; Thiagarajan et al., 2014).

Temperature reconstructions can help assess how well models simulate the subsurface response to deglacial AMOC variability and greenhouse gas rise. Reconstructions suggest that the tropical thermocline warmed during HS1 and the YD (e.g., Schmidt et al., 2012), as did the shallow (< 200 m) subpolar North Atlantic (Max et al., 2022). Several bottom water temperature (BWT) reconstructions suggest the subsurface North Atlantic above ~ 1500 m warmed during HS1 and/or the YD. For example, high Mg/Ca values in the calcitic benthic foraminifera genus *Uvigerina* may imply warming at ~ 850 m (within modern AAIW depths) in the tropical western Atlantic during HS1 and around the time of the YD (Poggemann et al., 2018). High Mg/Ca values in calcitic benthic foraminifera may also imply warming at ~ 1300 m (below modern AAIW) in the eastern equatorial Atlantic during these events (Weldeab et al., 2016a) and in the subpolar North Atlantic at ~ 1300 m during HS1 (Marcott et al., 2011). However, the Mg/Ca of benthic foraminifera is affected by changes in the carbonate ion saturation state ($\Delta[CO_3^{2-}]$), not only temperature (e.g., Elderfield et al., 1996, 2006; Yu & Elderfield, 2008). Geochemical evidence suggests higher $\Delta[CO_3^{2-}]$ during the LGM than the Holocene above ~ 2 km in the subpolar North Atlantic (e. g., Yu et al., 2010; 2019) and above ~ 1.5 km in the tropical Atlantic (Oppo et al., 2018; Yu et al., 2010), which could cause LGM temperature estimates based on Mg/Ca of benthic foraminifera to be too high. Several of these reconstructions (e. g., Yu et al., 2010; 2019) suggest a $\Delta[CO_3^{2-}]$ decrease from the LGM to HS1, but none clearly resolve variability across all deglacial millennial events, so the potential impact of such variations on Mg/Ca-based BWT reconstructions has not been assessed.

Recent work suggests that for the aragonitic foraminifera *Hoeglundina elegans,* dividing Mg/Ca by Li/Ca corrects for non-temperature effects on Mg/Ca (Bryan & Marchitto, 2008; Marchitto et al., 2018). The only published *H. elegans* Mg/Li-based deglacial BWT reconstruction from the North Atlantic is from the Florida Margin at modern AAIW depths, which shows warming during HS1 and the YD (Valley et al., 2019). However, at this location, changes in geostrophic flow related to AMOC variability cause vertical movement of isopycnals, and it is difficult to isolate this mechanism of temperature change from regional processes (Lynch-Stieglitz et al., 2014; Valley et al., 2017). Thus, *H. elegans*-based BWT records from other regions are needed to evaluate the effects of AMOC reduction, altered AAIW temperature, and greenhouse gas rise, on North Atlantic temperature within or near modern AAIW depths.

In addition to its influence on subsurface temperature, AMOC variability has a profound impact on subsurface nutrient distribution. Models suggest that on the millennial time scale, AMOC strength is tightly coupled to the northward extent of AAIW, an association explained by AAIW's role as part of the return flow that compensates for the export of North Atlantic Deep Water (NADW) at depth (e.g., Gu et al., 2017). AAIW is the main source of nutrients to the modern North Atlantic (e.g., Sarmiento et al., 2004; Tuerena et al., 2015), and so changes in its northern extent or composition in response to AMOC variability would alter the Atlantic's nutrient budget. For example, it has been suggested that a reduction in both AAIW's nutrient content and its northern extent contributed to the low nutrients in the glacial North Atlantic above ~ 2 km and in the glacial equivalent of NADW (Oppo et al., 2018).

Several studies support a link between a weak AMOC and reduced AAIW presence in the tropical Atlantic during the deglaciation (e. g., Came et al., 2008; Huang et al., 2014; Valley et al., 2017; Xie et al., 2012). Others argue against this association, suggesting that during deglacial events of reduced AMOC, AAIW advected more nutrients into the tropical North Atlantic (e. g., Poggemann et al., 2017). In addition to influencing the North Atlantic nutrient budget via its likely influence on AAIW northward extent, the AMOC intensity also influences the ventilation rate and the accumulation of remineralized organic matter. For example, model simulations suggest a weak AMOC results in enhanced accumulation of remineralized nutrients and carbon in the mid-depth North Atlantic (e. g., Gu et al., 2021; Schmittner & Lund, 2015; Yu et al. 2022).

In this study, we present new records spanning the LGM through mid-Holocene from a tropical western North Atlantic site within the depths of modern AAIW. We compare our new *H. elegans* Mg/Li-based BWT reconstruction to the two other published Atlantic *H. elegans* Mg/Li-based BWT reconstructions from AAIW depths – the Florida Margin site (Valley et al., 2017), and a site from the Brazil Margin (Umling et al., 2019). Similarly, to evaluate nutrient gradients between sites, we compare reconstructions of seawater Cd (CdW), which is correlated to phosphate concentration (e.g., Boyle, 1988), from the same sites. These comparisons help us evaluate the hypothesis that the western tropical North Atlantic at AAIW depths experienced regional warming during HS1 and the YD, independent of large local vertical displacement of isopycnals as occurs with reduced geostrophic transport at the Florida Margin (Lynch-Stieglitz et al., 2014; Valley et al., 2017). Evolution of temperature and nutrient gradients also provide insights into mechanisms of warming and nutrient variability.

We present new *Uvigerina peregrina* and *Cibicidoides pachyderma* Mg/Ca, Li/Ca, and Mg/Li core-top data, supplementing the B/Ca and Cd/Ca published previously (Oppo et al., 2018). New core-top *H. elegans* Mg/Ca, Li/Ca, Mg/Li, and Cd/Ca are also presented. The microhabitats of *C. pachyderma* and *H. elegans* are typically epifaunal (e. g., Corliss, 1991) or very shallow infaunal (within top 1 cm) (e.g., Fontanier et al., 2006) whereas *U. peregrina* is typically shallow infaunal (top 2 cm) (Corliss, 1991; Fontanier et al., 2006). We present new downcore elemental ratio records (Mg/Ca, Li/Ca, Mg/Li, Cd/Ca, B/Ca) from core KNR197-3-46CDH for the three species of benthic foraminifera – the aragonitic *H. elegans* and the calcitic foraminifera, *U. peregrina* and *C. pachyderma*. Cd/Ca records of all three species have been used to estimate the Cd concentration of seawater (e.g., Boyle, 1992; Boyle et al., 1995).

We discuss differences among the Mg/Ca downcore records generated on the three species in the context of our new *C. pachyderma* B/Ca data, which, like other species of *Cibicidoides* (Yu & Elderfield, 2008), can be used to estimate carbonate saturation state ($\Delta[CO_3^{2-}]$) (Oppo et al., 2018).

We compare Mg/Ca-based and Mg/Li-based BWT estimates of the calcitic species, using local calibrations, to the Mg/Li-based BWT estimate of the aragonitic species *H. elegans*, using an updated calibration that includes new core-top data. Some BWT reconstructions use clumped isotopes in solitary deep-sea corals (Hines et al. 2019; Thiagarajan et al. 2014), but to our knowledge, no tropical or North Atlantic data have been published from sites shallower than 1400 m (e. g., near or within AAIW depths) for the last deglaciation, so clumped isotope data are not discussed here.

2 Materials and Methods

We present elemental ratio data from a depth transect of multi-core tops (338 to 3328 m) from the Demerara Rise, western tropical North Atlantic, and downcore records from KNR197-3-46CDH (7°50'N, 53°40'W; hereafter 46CDH), recovered from ~950 m on the Demerara Rise. As discussed previously (Oppo et al., 2018), the influence of southern-sourced waters between ~ 400 and 1000 m on the Rise (here, referred to collectively as "AAIW") is evident from the relatively low salinities compared to overlying and underlying South Atlantic Central Waters and northern-sourced waters, respectively (Figure 1).

AAIW has higher phosphate (Brainbridge, 1981) and cadmium (Middag et al., 2018) and lower $\delta^{13}C$ of dissolved inorganic carbon (Kroopnick, 1985) and carbonate saturation state ($\Delta[CO_3^{2-}]$) (Yu et al., 2008) than North Atlantic waters from similar depths. Whereas North Atlantic waters are formed from nutrient-depleted surface and thermocline waters, AAIW begins its journey to the tropical Atlantic already containing upwelled, nutrient-rich waters. In addition, poor ventilation and the addition of respired nutrients and carbon intensify the North Atlantic tropical phosphate (and cadmium) maximum and $\delta^{13}C$ and $\Delta[CO_3^{2-}]$ minima (e.g., Duteil et al. 2012; Gebbie, 2014). Thus, in addition to changes in the relative proportion of AAIW and northern-sourced waters, past changes in CdW, $\delta^{13}C$, and $\Delta[CO_3^{2-}]$ at our Demerara Rise site may reflect changes in remineralized components, as well as preformed changes (e.g., Lynch-Stieglitz et al., 2019; Oppo et al., 2018; Poggemann et al., 2017; Weldeab et al. 2016a; Yu et al., 2008). Preformed changes can result in decoupling among these properties (e. g., Lynch-Stieglitz et al., 2019; Yu et al., 2008).

We compare our new BWT and CdW reconstructions to published *H. elegans*-based reconstructions from two other sites also recovered from depths affected by modern AAIW: Brazil Margin site KNR159-5-90GGC (1105 m) (Umling et al., 2019) and Florida Margin site (~550 m)

KNR166-2-26JPC (Valley et al., 2017, 2019) (red circles, Figure 1; Table 1). Finally, we discuss *Uvigerina* species Mg/Ca and Cd/Ca records from core M78/1-235-1 (Poggemann et al., 2017, 2018), recovered from ~ 850 m in the Tobago Basin (~11.6°N), also within modern AAIW (Figure 1**,** yellow triangle) in the context of our new records.

The influence of relatively low-salinity AAIW at the core sites decreases from south to north (Figure 1). The Brazil Margin site of KNR159-5-90GGC, most influenced by AAIW, is located just below the low salinity core of AAIW. AAIW and shallower southern-sourced waters still dominate (~70%) the water mass mixture at ~ 950 m on the Demerara Rise (Oppo et al., 2018). Waters at the Tobago Basin site of M78/1-235-1 are both warmer and saltier (5.4°C, 34.73 psu) than at the Demerara Rise site (5.0°C, 34.62 psu), indicating further dilution of AAIW by northern-sourced waters. AAIW also contributes to waters along the Florida Margin (Szuts & Meinen, 2017), where KNR166-2-26JPC was recovered. However, relatively warm and salty waters (7.0°C, 34.9 psu; Bryan & Marchitto, 2010) are consistent with further dilution of the AAIW core with subtropical waters compared to the sites farther south.

2.1 Elemental ratio measurements

Foraminifera were cleaned following the full trace metal protocol (Boyle & Keigwin, 1985; Boyle & Rosenthal, 1996). Core-top *U. peregrina* and *C. pachyderma* data and downcore *C. pachyderma* data were collected at the Woods Hole Oceanographic Institution (WHOI) on a Thermo-Finnigan Element2 sector field single-collector inductively coupled plasma mass spectrometer (ICP-MS) following the method of Rosenthal et al. (1999) and subsequent modifications (Huang et al., 2008; Lear et al., 2002; Marchitto, 2006). Following the same methods, downcore *U. peregrina* and some downcore *H. elegans* data were generated at the Institute of Earth Sciences, Academia Sinica, on a Thermo Scientific Element XR sector field single-collector ICP-MS. The remaining downcore *H. elegans* data and all *H. elegans* core-top data were generated at the WHOI on a Thermo Scientific iCAP quadrupole ICP-MS (iCAP Q). Inter-laboratory calibrations were conducted to assess the presence of laboratory offsets. A summary of where each data set was collected, and which corrections, if any, were applied is provided in Table S1 in Supporting Information SI.

To align WHOI data with published Mg/Li and Cd/Ca data on *H. elegans*, several measurements were made on foraminifera from the same core-top samples as published in Bryan & Marchitto (2008), and several WHOI iCAP Q standards and an international limestone standard were measured on a Thermo Element2 at the Institute of Arctic and Alpine Research, University of Colorado, Boulder, Colorado (INSTAAR) (Text S1 and Table S2 in the Supporting Information SI). Similarly, an inter-laboratory calibration was conducted between the WHOI iCAP Q and IES Element XR, using standards and including some splits of the same crushed, homogenized, downcore samples (Text S2 and Table S3 in the Supporting Information S1). Adjustments were necessary to correct for laboratory offsets (Figures S1-S4 in Supporting Information S1).

Precision was monitored with matrix-matched standards. Long-term precision (2σ) was better than 3% for all elements measured on the Academia Sinica Element XR and for Mg/Ca, Li/Ca, and B/Ca measured on the WHOI Element2, and better than 2% for Mg/Ca and Li/Ca measured on the INSTAAR Element2. Long-term precision for Cd/Ca measured on the Element2 was 5% at both WHOI and INSTAAR. Long-term precision (2σ) on the iCAP Q for three to four consistency standards having similar ratios to *H. elegans* (0.27-1.52 mmol/mol, 1.31-4.35 μmol/mol, 0.05-0.08 μmol/mol, and 28-54 μmol/mol, for Mg/Ca, Li/Ca, Cd/Ca, and B/Ca respectively), run across a range of calcium concentrations (60-150 ppm), and averaged after applying the same matrix correction applied to unknowns, was 0.04 mmol/mol (5.5%), 0.10 μmol/mol (4%), 0.005 μmol/mol (8%), and 4 μmol/mol (11%) for Mg/Ca, Li/Ca, Cd/Ca, and B/Ca respectively. The relatively low precision expressed as percentage is the result of the relatively low molar ratios of the consistency standards. The precision, expressed as a molar ratio, is comparable to that of the other laboratories.

2.2 Chronologies

We used the Bayesian statistical package "BACON" (Blaauw & Christen, 2011) in R and the Marine20 calibration (Heaton et al., 2020) to update the chronology for 46CDH, and for KNR166-2-26JPC and KNR159-5-90GGC from the Florida Margin and Brazil Margin, respectively. We use a marine reservoir correction DeltaR= -100±200 years. This correction is approximated from data near the sites of KNR166-2-26JPC (-45±51 years; one estimate near core site) and KNR159-5-90GGC (-87±38 years; five nearest values), as summarized on the Calib 8 webpage (http://calib.org/calib/). There are no reservoir ages reported in the vicinity of the Demerara Rise, so in the absence of evidence to the contrary, we also use DeltaR= -100±200 years.

For KNR197-3-46CDH, we use dates from Huang et al. (2014) as well as a few new dates (Data Set 1 in Supporting Information S1). As in previous studies, we omit a few anomalously young dates (one of two dates at 166.5 cm, and both dates at 200.5 cm). We also omit a date at 224.5 cm, which falls below the line connecting the older of the two dates at 166.5 cm and the next deepest date at 233.5 cm, suggesting that the sample from 224.5 cm may also contain planktic foraminifera that were bioturbated from overlying younger sediment. As a result, our radiocarbon-based chronology is poorly constrained between ~ 9 and 14 ka (Figure S5). To improve the chronology in the critical, early part of this interval, we compared the benthic $\delta^{18}O$ record from KNR197-3-46CDH (Oppo et al., 2018), on the ensemble median age time scale, to that of nearby core KNR197-3-25GGC (7.63°N, 53.79°W, 671 m) (Data Set S2 in Supporting Information SI), which does not contain radiocarbon reversals (Data Set S1 in Supporting Information SI). In KNR197-3-25GGC, the peak of the brief $\delta^{18}O$ increase superimposed on the deglacial trend of decreasing $\delta^{18}O$ corresponds to the Bølling. We thus replaced the radiocarbon constraint from the 233.5 cm (having a mean ensemble age of ~ 14.25 ka) with a new benthic $\delta^{18}O$-based depth-age constraint (Figure S5 in Supporting Information SI).

For KNR159-5-90GGC, we use dates from Lund et al. (2015), Umling et al. (2019) and Yu et al. (2022). Following these previous studies, we omit most dates collected on planktic foraminifera between 80 and 150 cm from KNR159-5-90GGC, as well as a date from 72.5 cm. Lund et al.'s (2015) hypothesis that young planktic foraminifera were preferentially bioturbated down core compared to benthics was confirmed with dates on planktic and benthic foraminifera from the same depths (Yu et al., 2022) and supports the chronology used in this study. For KNR-166-2-26JPC we use radiocarbon dates published in Lynch-Steiglitz et al. (2014). The similarity of the BWT and CdW reconstructions from the Demerara Rise and Florida Margin, discussed in Section 5, supports our chronology for the Demerara Rise site between ~9 and 14 ka, which, as noted above, is poorly constrained.

2.3. Age uncertainty analyses

To take age uncertainty into consideration, we use an R package "geoChronR" (McKay et al. 2021) to model, analyze, and visualize the age-uncertain proxy data. For each core, we first created an age model using the `runBacon` function, then created 1,000 age-uncertain proxy ensembles in each core, computed the median ensemble member and the 50% and 95% highest-density probability ranges in each proxy, and exported the ensemble series using `plotTimeseriesEnsRibbons` function.

The plotting of outliers on the age axis was set to exclude values below 5% and 95% probability limit (`limit.outliers.x = 0.025`). We exported the raw downcore data with their median BACON age. Files to reproduce the results are in the Supporting Information SI.

3 Results

3.1 Core-top Data

Carbonate saturation state and other environmental factors related to the biocalcification process affect the Mg/Ca and Li/Ca of benthic foraminifera (e.g., Bentov et al., 2009; Bentov and Erez, 2006; Bryan & Marchitto, 2008; de Nooijer et al. 2009; Elderfield et al., 1996, 2006; Erez, 2003; Hall & Chan, 2004; Marriott et al., 2014; Marchitto et al., 2018; Martin et al., 2002; McCorkle et al., 1995; Nürnberg et al., 1996; Yu & Elderfield, 2008). Both Li/Ca and Mg/Ca have low calcite and aragonite abiotic partition coefficients (<<1) (Gaetani & Cohen, 2006; Marriott et al., 2004; Oomori et al., 1987). This implies that calcification discriminates against the incorporation of Li and Mg and so the Li/Ca and Mg/Ca of the foraminifera are lower than the ratio within the calcifying fluid. Assuming a closed or semi-enclosed calcifying pool, such discrimination would lead to increases in Mg/Ca and Li/Ca in the residual calcifying fluid (Elderfield et al., 1996). This effect is greater at lower $\Delta[CO_3^{2-}]$ than higher $\Delta[CO_3^{2-}]$ due to the effect of $\Delta[CO_3^{2-}]$ on precipitation rate and so, if this were the only influence on the ratios, Mg/Ca and Li/Ca should be positively correlated to $\Delta[CO_3^{2-}]$. Increased pumping of Ca^{2+} into the calcifying fluid at low $\Delta[CO_3^{2-}]$ would also cause such a correlation (Marchitto et al., 2018). Inorganic precipitation experiments suggest temperature also influences these ratios in calcite and aragonite: Mg/Ca increases and decreases with increasing temperature in calcite and aragonite, respectively, whereas Li/Ca decreases with increasing temperature in both (Gaetani & Cohen, 2006; Marriott et al., 2004; Oomori et al., 1987).

New and published (Oppo et al., 2018) Demerara Rise Mg/Ca and Mg/Li core-top data for *C. pachyderma, U. peregrina*, and *H. elegans* (Data Set S3 in Supporting Information SI) are shown versus BWT on Figure 2, and versus carbonate saturation state in Figure S6 in Supporting Information S1. Core-top Li/Ca data are also shown in Figure S6 in Supporting Information S1. Core-top Li/Ca of *C. pachyderma* is weakly negatively correlated to BWT (R^2=0.02). Li/Ca of *U. peregrina* is also negatively correlated to BWT (R^2=0.37), whereas Li/Ca in *H. elegans* is positively correlated (R^2=0.65). Li/Ca of all three species (and other calcitic species) is negatively correlated to BWT in core tops from the Florida Strait (Bryan & Marchitto, 2008), consistent with our data on calcitic foraminifera but not with our *H. elegans* data. However, a positive trend for *H. elegans* emerged at low temperatures with the addition of new data (Marchitto et al., 2018), and our data are consistent with those data. Li/Ca in *H. elegans* from the Demerara Rise core tops is lower than published data from similar temperatures (Figure S7 in Supporting Information SI), likely due to the lower aragonite saturation state at the Demerara Rise.

Core-top Mg/Ca values of all three species exhibit positive correlations to BWT (*C. pachyderma*: R^2=0.90; *U. peregrina*: R^2=0.87; and *H. elegans*: R^2= 0.89) (Figure 2). The local core-top calibration equation for *C. pachyderma* is $Mg/Ca=0.150\pm0.018*BWT + 0.356\pm0.103$, and for *U. peregrina* is $Mg/Ca=0.080\pm0.009*BWT + 0.780\pm0.049$. Our Mg/Ca-BWT data overly Florida Strait *C. pachyderma* data presented in Bryan & Marchitto (2008), although their data extend to warmer temperatures, resulting in a different core-top calibration. Our calibration equation for *U. peregrina* is nearly identical to theirs from the Florida Strait. On the other hand, our *H. elegans* Mg/Ca values are lower than published data from similar temperatures (Figure S7 in Supporting Information SI), likely due to the lower aragonite saturation state.

Li/Ca is positively correlated to $\Delta[CO_3^{2-}]$ for all three species (*C. pachyderma*: R^2=0.81; *U. peregrina*: R^2= 0.40; and *H. elegans*: R^2= 0.31) (Figure S6 in Supporting Information SI). The correlation between $\Delta[CO_3^{2-}]$ and benthic foraminiferal Li/Ca in the Norwegian Sea is also positive (Lear et al., 2006), but negative in the Florida Strait (Bryan & Marchitto, 2008). The positive correlation between $\Delta[CO_3^{2-}]$ and Li/Ca at Demerara Rise is consistent with the hypothesis that in relatively low $\Delta[CO_3^{2-}]$ environments (like the Demerara Rise and Norwegian Sea), the effect of $\Delta[CO_3^{2-}]$ dominates over the temperature effect on Li/Ca, whereas the temperature influence may be more dominant in higher−$\Delta[CO_3^{2-}]$ environments (Bryan & Marchitto, 2008; Doss et al., 2018).

Demerara Rise core-top Mg/Ca is uncorrelated to $\Delta[CO_3^{2-}]$ except for *H. elegans*, which is positively correlated (R^2= 0.20) (Figure S6 in Supporting Information SI). *H. elegans* Mg/Ca values are similar to values in other areas with low temperatures and low aragonite saturation state, where they are also positively correlated to $\Delta[CO_3^{2-}]$ (Rosenthal et al., 2006). *H. elegans* core-top B/Ca is positively correlated to aragonite saturation state (R^2=0.45; not shown), consistent with previous work (Yu & Elderfield, 2007).

Core-top Mg/Li is positively correlated to BWT for all three species (*C. pachyderma*: R^2=0.90, *U. peregrina*: R^2= 0.86, *H. elegans*: R^2= 0.77) (Figure 2). The local core-top calibration equations are $Mg/Li= 0.0126\pm0.0015*BWT + 0.0285\pm0.0086$ for *C. pachyderma* and $Mg/Li=0.0076\pm0.0010*BWT + 0.0417\pm0.0049$ for *U. peregrina*. The relationships at the Demerara Rise are similar to published *U. peregrina* data (Bryan & Marchitto, 2008), but for *C. pachyderma*, are offset to lower Mg/Li at relatively cold BWT. The Mg/Li-BWT relationship of *H. elegans* is similar across sites (Marchitto et al., 2018), and we combine new and published data (Data Set S4 in Supporting Information SI) to develop a new linear Mg/Li-BWT calibration (Figure 3).

$$\mathrm{Mg/Li} = 0.1794(\pm0.0037) + 0.01484(\pm0.0003) \times \mathrm{BWT}\ (R^2 = 0.93) \qquad (1)$$

The standard error of temperature estimates is ±1.4 °C with a Mg/Li standard error of estimate of ±0.02 mol/mmol. Compared to the original equation (Marchitto et al., 2018), the new calibration suggests slightly colder temperatures at low Mg/Li and slightly warmer temperatures at high Mg/Li. More core-top data would be useful to further constrain the relationship between Mg/Li and BWT.

CdW estimates for *H. elegans* using Boyle's (1995) distribution coefficient for this species (D=1) returns CdW estimates similar to seawater cadmium measured at the Demerara Rise (Figure S8 in Supporting Information SI). By contrast, applying Boyle's (1992) depth-dependent distribution coefficient for calcitic foraminifera to *C. pachyderma* and *U. peregrina* Cd/Ca overestimates seawater cadmium at the Demerara Rise (Oppo et al., 2018) (Figure S8 in Supporting Information SI).

3.2 Downcore Data

In this section, we discuss LGM to mid-Holocene (MH; here ~6 -7 ka) trends in the elemental ratio records from KNR197-3-46CDH (Data Set S5 in Supporting Information SI). We present records versus depth, to maintain focus on the difference between species, rather than on interpretation of millennial-scale features of the deglaciation.

3.2.1 Multispecies B/Ca Records

A decrease in B/Ca values from the LGM to the MH is evident in all three species, with B/Ca decreasing by ~ 40, 20, and 5 µmol/mol in *C. pachyderma*, *H. elegans* and *U. peregrina*, respectively (Figure 4a). As core-top B/Ca values of *C. pachyderma* (Oppo et al., 2018), *Uvigerina,* and *H. elegans* (Yu & Elderfield, 2007) are correlated to and likely controlled by $\Delta[CO_3^{2-}]$ (Yu and Elderfield, 2007), the results imply higher glacial than Holocene $\Delta[CO_3^{2-}]$ in bottom and shallow pore waters. Our finding of smaller glacial-Holocene B/Ca decreases in *U. peregrina* and *H. elegans* than *C. pachyderma* is consistent with the higher sensitivity of *Cibicidoides* species to $\Delta[CO_3^{2-}]$ indicated in previous studies of B/Ca of benthic foraminifera from core-top sediment (e. g., Rae et al., 2011; Yu & Elderfield, 2007).

3.2.2 Multispecies Li/Ca, Mg/Ca, and Mg/Li Records

Li/Ca values of all three species also exhibit glacial-Holocene decreases (Figure 4b). The parallel decline with B/Ca is consistent with a strong influence of $\Delta[CO_3^{2-}]$ on Li/Ca via the biomineralization process, as suggested previously (Hall & Chan, 2004; Lear & Rosenthal, 2006; Marchitto et al., 2018). Assuming that waters at the site warmed during the deglaciation, the trends are also consistent with an inverse relationship between temperature and Li/Ca (Hall & Chan, 2004; Marriott et al, 2004).

Mg/Ca values of *C. pachyderma* and *H. elegans* also exhibit clear glacial-Holocene decreases (Figure 4c). If interpreted only as BWT signals based on the core-top relationships, these Mg/Ca trends would imply warmer glacial than Holocene temperatures at the core site. The Mg/Ca of *U. peregrina* has a more complex signal, with similar LGM and Holocene values, and highest values in between. Given the likelihood that this site warmed during the deglaciation, the similar trends of B/Ca and Mg/Ca in *H. elegans* and *C. pachyderma* suggest that the LGM to MH Mg/Ca decreases are dominated by a decrease in $\Delta[CO_3^{2-}]$, and not by temperature. This finding is consistent with previous work that suggests that variations in Mg/Ca values of two other *Cibicidoide*s species (*C. wuellerstorfi* and *C. mundulus*) are dominated by $\Delta[CO_3^{2-}]$ effects (Yu & Elderfield, 2008). The similar LGM and MH *U. peregrina* Mg/Ca values also suggest a $\Delta[CO_3^{2-}]$ influence.

We compare Mg/Ca-based and Mg/Li-based BWT estimates of the calcitic foraminifera to the *H. elegans* Mg/Li-based estimate, converted to BWT using Equation (1). We use local core-top calibrations to convert Mg/Ca of *U. peregrina* and the Mg/Li (Figure 4d) to BWT. We do not convert the Mg/Ca of *C. pachyderma*, as the results would suggest much warmer glacial than

Holocene temperatures. The *H. elegans* reconstruction suggests late glacial/early deglacial temperatures of about 3°C, peaking above 8°C, and cooling to about 5.5°C by the MH (Figure 4d). The deglacial *U. peregrina* Mg/Ca-BWT reconstruction suggests peak warmth at about the same time as the *H. elegans* Mg/Li-BWT reconstruction, consistent with a strong buffering of $\Delta[CO_3^{2-}]$ within pore waters in shallow sediments where *Uvigerina* calcify (Elderfield et al., 2006, 2010). However, the similar LGM and MH *U. peregrina* Mg/Ca (and Mg/Ca-based BWT estimates), along with the decreasing LGM-MH trends of B/Ca and Li/Ca (which are correlated; R^2=0.83; not shown) suggest that buffering in shallow pore waters is not always complete, consistent with previous evidence (Weldeab et al., 2016b). We thus suggest that the similar LGM and MH *U. peregrina* Mg/Ca are likely due to higher LGM than MH $\Delta[CO_3^{2-}]$ in shallow pore waters, and do not reflect similar BWTs.

The application of the local Mg/Li calibrations (Section 3.1) to the downcore *U. peregrina* and *C. pachyderma* confirms that the influence of $\Delta[CO_3^{2-}]$ on Mg/Ca is at least partly corrected for by dividing by Li/Ca (Bryan & Marchitto, 2008). However, *C. pachyderma* Mg/Li suggests a small range of BWT variability (~ 2°C), thus underestimating BWT variations reconstructed from Mg/Li of *H. elegans* (Figure 4d). BWT estimated from Mg/Li of *U. peregrina* shares some features of the *H. elegans*-based BWT reconstruction, especially above ~ 225 cm. However, from ~ 300 to 225 cm, *Uvigerina* Mg/Li often underestimates BWT by ~ 2-3°C. Given errors of about ±1.5°C the two reconstructions are within error of each other, even during the interval of differences in the best estimate. If additional studies demonstrate that the core-top relationship between *U. peregrina* Mg/Li and BWT holds across many different environments, and *U. peregrina* Mg/Li-BWT calibrations replicate *H. elegans* Mg/Li-based BWT estimates, this would bolster confidence in the use of *U. peregrina* Mg/Li to reconstruct BWT. However, as *H. elegans* Mg/Li appears to record BWT across a range of environments, and its relationship to temperature also appears consistent with that in coral aragonite (Marchitto et al., 2018), here we use the *H. elegans* Mg/Li-based BWT reconstruction.

3.2.3 Multispecies Cd/Ca Records

LGM Cd/Ca values are lower than MH values for all three species though the trend is most pronounced in *U. peregrina* and least pronounced in *H. elegans* (Figure 4e). The records of all three species show a deglacial oscillation towards lower values. The generally higher Cd/Ca values for *U. peregrina* than *C. pachyderma* are consistent with the core-top data from the Demerara Rise, also showing values 0.01 to 0.02 µmol/mol higher in *U. peregrina* (Figure S8 in Supporting Information S1).

We convert Cd/Ca to CdW using the published distribution coefficient (D=1) for *H. elegans* (Boyle et al. 1995) and the depth-dependent distribution coefficient (D=1.3) (Boyle, 1992) for the calcitic species. The Mid-Holocene CdW estimates for calcitic foraminifera from 46CDH are similar to modern, contrasting with multi-core top data (Figure S8a in Supporting Information S1). *H. elegans* and *C. pachyderma* CdW reconstructions are similar above ~270 cm, but *C. pachyderma* estimates are generally lower below ~270 cm. The *U. peregrina* record is generally offset to higher CdW estimates (Figure 4f). Applying the higher distribution coefficient (D=1.8) for calcitic foraminifera from Oppo et al. (2018) brings the downcore *U. peregrina*-based estimates closer to the *H. elegans* estimates but the *C. pachyderma*-based estimates lower than the *H. elegans*-based estimates (not shown).

Along with the core-top offsets (Oppo et al., 2018) (Figure S8 in Supporting Information S1) these results seem to imply different Cd/Ca distribution coefficients for *U. peregrina* and *C. pachyderma*, although evidence from other sites exists to the contrary (Boyle, 1992; Bryan & Marchitto, 2010). Typical *U. peregrina* Mn/Ca in 46CDH is 40-80 µmol/mol whereas that of *C. pachyderma* is 60-120 µmol/mol, suggesting that manganese carbonate overgrowths are not the reason for the relatively high Cd/Ca *U. peregrina* values. Another possibility that we cannot test with samples in hand is that higher pore water concentrations gave rise to the higher *U. peregrina* Cd/Ca value compared to the other species.

When it is available, *H. elegans* is generally preferred for CdW because it has a smooth glassy test, making it less prone to manganese carbonate overgrowth, and thus, less prone to contamination (Boyle, 1995). However, given the uncertainty in the CdW reconstructions, and the similarity of the *H. elegans* and *C. pachyderma* Cd/Ca for most of the study interval, we consider both reconstructions in our discussions. For consistency with published records, and because they return CdW estimates that are similar to each other (Figure 4f), we use Boyle's (1992) calcitic (D = 1.3) and Boyle et al.'s (1995) *H. elegans* distribution coefficients (D = 1).

4 Subsurface Variability Recorded in KNR197-3-46CDH

The reconstructions from Demerara Rise core 46CDH show large glacial-Holocene trends, as well as millennial-scale variability associated with North Atlantic deglacial climate oscillations (Figure 5). Compared to the mid-Holocene, the LGM at our western tropical Atlantic site was ~3°C colder, nutrient depleted, and had higher $\Delta[CO_3^{2-}]$. Using the core-top relationship between $\Delta[CO_3^{2-}]$ and B/Ca of *C. pachyderma* (Oppo et al., 2018), we estimate that glacial $\Delta[CO_3^{2-}]$ was ~ 100 μmol/kg, or ~ 30-40 μmol/kg higher than the MH (Figure 5b). The glacial value is comparable to values found today in the deep subtropical thermocline (e.g., 150-100 μmol/kg between 250 and 550 m at the Great Bahama Banks; Bryan & Marchitto, 2008) and to glacial values at ~1150 m in the subpolar North Atlantic (Yu et al., 2019). The relatively low CdW and high glacial $\Delta[CO_3^{2-}]$ are consistent with a greater contribution of northern-sourced waters at the expense of AAIW to the site during the LGM (Oppo et al., 2018).

The Demerara Rise $\Delta[CO_3^{2-}]$ began a long-term decrease at ~ 17 ka. Four factors may have contributed to the glacial-Holocene decline: (1) decreasing "endmember" $\Delta[CO_3^{2-}]$ values of northern surface source waters due to rising atmospheric CO_2 (Yu et al., 2008), (2) decreasing $\Delta[CO_3^{2-}]$ of AAIW after about 16 ka (Lacerra et al., 2019), (3) an LGM-to-Holocene decrease in the contribution of high-$\Delta[CO_3^{2-}]$ northern-sourced waters relative to low-$\Delta[CO_3^{2-}]$ AAIW, and (4) greater accumulation of respired material in the ocean interior along the water mass pathways to the site. CdW increased from the LGM to the Holocene, implying that at least some component of the $\Delta[CO_3^{2-}]$ decrease was due to increasing southern waters and/or enhanced accumulation of remineralized organic matter, that is the 3rd and/or 4th mechanisms.

On the millennial time scale, CdW also generally varied with a sign opposite to $\Delta[CO_3^{2-}]$ (Figure 5e) implying that variations in remineralized organic matter, either preformed or accumulated along water mass flow paths or within the tropics, contributed to these oscillations. As discussed in Section 5.2, AMOC variability likely contributed to the observed millennial-scale $\Delta[CO_3^{2-}]$ and CdW variations.

Only one glacial sample had enough *H. elegans* to measure elemental ratios, so additional data are needed to establish the onset of initial warming. Regardless of the timing of initial warming, BWT rose from ~17.4 ka through HS1 (Figure 5c). Aside from a brief cooling during the warm peak of the BA (during the Bølling), which is also evident in the benthic $\delta^{18}O$ record (Figure 5e), warming continued until the beginning of the YD, remained approximately constant during the YD, then began a long-term cooling that continued to at least ~6 ka.

5 Comparison to other Atlantic *H. elegans* records from AAIW depths

5.1 Deglacial Temperature Variability at modern AAIW depths

The Demerara Rise (950 m core depth) BWT reconstruction (Figure 5) provides clear evidence of warming during HS1 in the western tropical North Atlantic at modern AAIW depths, independent of isopycnal tilt variations as may have occurred at the Florida Margin in response to variability in geostrophic flow (Lynch-Stielglitz et al., 2014; Valley et al., 2019). As discussed in Section 1, model simulations suggest that if reduced vertical mixing dominates over reduced northward heat advection when the AMOC weakens, subsurface warming occurs in northern high-latitude convection regions and along the upper AMOC return flow path, where our site is located (e.g., He et al., 2020; Liu et al., 2009; Pedro et al., 2018). Single forcing simulations suggest that the deglacial atmospheric CO_2 rise also causes a subsurface warming response in the upper North Atlantic during HS1 (see Figure 6 in Umling et al., 2019), and both mechanisms likely contributed to early HS1 warming at our site.

We apply Equation (1) to two published *H. elegans* Mg/Li records (Valley et al. 2019; Umling et al., 2019) to update BWT estimates. Due to the scarcity of glacial data, we cannot identify the time of initial HS1 warming at the Demerara Rise, but by ~17 ka, warming was underway. This warming was approximately simultaneous with warming at the Florida Margin, where warming began at ~18 ka (550 m; Valley et al., 2019) (Figure 6). BWTs at the two sites were within error of each other from ~17 ka to ~12 ka, whereas in the modern, the Demerara Rise site is colder, reflecting a greater proportion of relatively cold AAIW at the Demerara Rise. The similar deglacial temperatures at the two sites during HS1 may imply a similar water mass mixture of northern and southern sources.

The Brazil Margin BWT reconstruction suggests that South Atlantic water at AAIW depths may have warmed by as much as 0.5°C before 16.5 ka. By this time, the tropical sites had already experienced significant warming (~4°C at the Florida Margin, and at least ~2.5°C at the Demerara Rise). The greater warming between 18 ka and 16.5 ka at the tropical sites implies that this warming was not transferred from the Southern Ocean to the tropics via AAIW. Instead, this earlier and larger warming at the Demerara Rise and Florida Margin compared to the Brazil Margin is consistent with warming mechanisms suggested from modeling studies – deglacial CO_2 rise and AMOC reduction (e.g., Liu et al., 2009; Umling et al., 2019). Isopycnal deepening may have also contributed to warming at the Florida Margin (Lynch-Stieglitz et al., 2014). However, the Brazil Margin warmed by ~3°C from ~16.5 to 14. 5 ka, implying that AAIW may have contributed to late HS1 warming in the tropical Atlantic, as suggested by Poggemann et al (2018).

Like the Demerara Rise, the Florida Margin was colder early in the BA (during the Bølling) than during the peak warmth of HS1 (Figures 5c and 6b). Such a brief cooling is consistent with a reinvigoration of the AMOC, which would result in northward transport of accumulated heat away from the tropics (e. g. Pedro et al., 2018). Cooling at the Florida Margin may have been larger due to the associated shoaling of isopycnals. The cooling was short lived, however, as both sites warmed during the rest of the BA (during the Allerød). Atmospheric CO_2 decreased by ~2 ppm during the Allerød (Figure 6e), and so could not be the driver of continued warming. In the TraCE-21K ice-sheet single-forcing simulation, orographic effects of a diminishing ice sheet drive an AMOC reduction (Zhu et al., 2014), resulting in significant subsurface warming from the Bølling through the beginning of the YD (Umling et al., 2019). As discussed in Section 6, our CdW reconstructions hint at such an AMOC weakening. A weaker AMOC and associated reduced northward surface heat transport is consistent with high-latitude North Atlantic regional cooling from the Bølling through the rest of the BA as reconstructed in ice cores (e.g., Kindler et al., 2014).

BWT at the Demerara Rise peaked during the late BA and YD, but warmth may have been the culmination of the Allerød warming, rather than specifically associated with the YD (Figures 5 and 6). YD warming at the Florida Margin may also have been the culmination of a longer-term trend, but the larger warming than at the Demerara Rise may indicate that deepening of isopycnals in response to reduced geostrophic flow contributed to the YD warming at the Florida Margin (Valley et al., 2019) (Figure 6b).

Our record does not provide evidence for subsurface cooling during the YD as simulated in TraCE-21K (Liu et al., 2009; Umling et al, 2019; He et al., 2020). The lack of a discernable BWT response may indicate a muted response to a relatively smaller AMOC weakening, and/or when an AMOC weakening begins from a stronger AMOC state. However, the absence of a discernible warming at the Demerara Rise specifically associated with the YD should be confirmed with BWT reconstructions from other tropical sites within AAIW depths, as our site may have been located near the boundary between southern warming and northern cooling that is simulated with a relatively modest AMOC reduction (e.g., He et al., 2020).

Cooling at the Demerara Rise between the end of the YD and the end of our record (~ 5 ka) may have resulted in part from cooling in the northern-source water endmember, as cooling is also observed at the Florida Margin, which presumably contained more waters of northern origin than the Demerara Rise, as is the case in the modern. A cooling trend is not evident at the Brazil Margin site, suggesting that cooling of AAIW was likely not the reason for the cooling trend. However, an increase in the fraction of cold AAIW relative to northern sources may have contributed to the Holocene cooling. The latter would imply a strengthening AMOC during this early-mid Holocene interval.

5.2 Deglacial $\Delta[CO_3^{2-}]$ and nutrient variability at modern AAIW depths

During the late LGM and HS1, $\Delta[CO_3^{2-}]$ at the Demerara Rise was higher than at the Brazil Margin site (Figure 6), providing strong evidence for a smaller contribution of AAIW to the Demerara Rise compared to the Holocene, when the $\Delta[CO_3^{2-}]$ gradient was small or absent, as in the modern. $\Delta[CO_3^{2-}]$ rose at the Brazil Margin site near the beginning of HS1 (Lacerra et al., 2019), probably due to outgassing of CO_2 in the South Atlantic sector of the Southern Ocean (Yu et al., 2022). There appears to have been little change in the Demerara Rise $\Delta[CO_3^{2-}]$ from the LGM to ~17 ka, and the relatively high $\Delta[CO_3^{2-}]$ and low CdW imply that northern source waters continued to dominate the water mass mixture at the Demerara Rise, even during early HS1.

From ~17 ka to ~16 ka, $\Delta[CO_3^{2-}]$ decreased gradually at the Demerara Rise site. Declining $[CO_3^{2-}]$ in northern source waters associated with rising atmospheric CO_2 (Yu et al., 2008) may have contributed to the $\Delta[CO_3^{2-}]$ decrease. However, CdW was also increasing at both the Demerara Rise and Florida Margin during this period, suggesting that at least some of the $\Delta[CO_3^{2-}]$ decrease was associated with an increase in respired organic matter, possibly transported southward from the North Atlantic source region, where it was likely accumulating due to a weak AMOC (e.g., Gu et al., 2021; Schmittner & Lund, 2015; Yu et al., 2019, 2022). Though 17-16 ka is generally considered a time of weak AMOC (e.g., McManus et al., 2004; Ng et al., 2018), we cannot independently rule out a gradual increase in AAIW in the water mass mixture at the site, which could also give rise to these signals. In addition, respired organic matter may have accumulated within the tropical phosphate maximum itself, as occurs in the modern ocean due to relatively weak ventilation (e. g., Duteil et al. 2012; Gebbie, 2014).

CdW increased abruptly at ~16 ka at the Florida Margin site (Figure 6d), which Valley et al. (2017) attributed to renewed incursion of AAIW into the western tropical Atlantic in response to strengthening of the upper branch of the AMOC. At the Demerara Rise, the *C. pachyderma*-based CdW increased abruptly at about the same time, although the *H. elegans*-based CdW increased abruptly earlier, approximately coincident with the initial $\Delta[CO_3^{2-}]$ decrease (Figure 5). Regardless, by ~16 ka, CdW at both sites was similar to CdW at the Brazil Margin, consistent with a strong presence of AAIW (Figure 6). The $\Delta[CO_3^{2-}]$ gradient between the Brazil Margin and Demerara Rise decreased, also consistent with a greater AAIW influence in the northern tropics. However, as CdW did not increase at the Brazil Margin site until the end of HS1, it is unlikely that the main cause of high nutrients in the tropical Atlantic at modern AAIW depths was an increase in the preformed nutrient content of AAIW (e. g., Poggemann et al., 2017).

Consistent with a more significant reinvigoration of the AMOC at the BA onset, the $\Delta[CO_3^{2-}]$ gradient between the Demerara Rise and the Brazil Margin sites collapsed (Figure 6), implying more AAIW at the Demerara Rise during the BA than late HS1. The abrupt increase in CdW at the Brazil Margin (Figure 6) also implies an expanded presence of AAIW into the South Atlantic at the BA onset (Umling et al., 2019; Yu et al., 2022). As discussed in section 5.1, cooling at the two tropical sites is also consistent with an AMOC reinvigoration. Neodymium isotope records from the Demerara Rise suggest an increase in the AAIW contribution (Huang et al., 2014), also supporting this explanation for the $\Delta[CO_3^{2-}]$ decrease at the BA onset.

During the YD, $\Delta[CO_3^{2-}]$ values between the Demerara Rise and Brazil Margin sites diverged, implying a retreat of AAIW and a weak AMOC. CdW values at both the Demerara Rise and Florida Margin were similar to subtropical North Atlantic values, also consistent with a relative increase in the northern source compared to southern sources (Came et al., 2008; Valley et al., 2017).

From the end of the YD to the end of our record (~ 5 ka), Demerara Rise $\Delta[CO_3^{2-}]$ decreased and CdW increased, both suggesting an increase in the proportion of AAIW relative to northern source waters, which could imply an AMOC strengthening. An abrupt atmospheric CO_2 increase at the end of the YD may have reduced $[CO_3^{2-}]$ of northern surface source waters, contributing to the initial $\Delta[CO_3^{2-}]$ decrease. However, cooling at the Demerara Rise from the end of the YD to ~ 5 ka is also consistent with an increasing proportion of AAIW. Tropical CdW values diverge from subtropical North Atlantic values (Came et al., 2008; Valley et al., 2017) and subpolar North Atlantic values (Bertram et al. 1995; Yu et al. 2007, 2019) (Figure S9 in Supporting Information SI), also consistent with increasing AAIW relative to northern source waters at the sites, and an AMOC strengthening. Although a Holocene decrease in CdW at the Florida Margin has been interpreted to indicate a weakening of the AMOC (Valley et al., 2022), much of the CdW decrease at the Florida Margin occurred after ~ 5 ka, so we do not rule out an early Holocene AMOC strengthening, followed by a later Holocene weakening.

At the Demerara Rise site, the early-to-mid Holocene trend of decreasing $\Delta[CO_3^{2-}]$ was interrupted by an abrupt increase in $\Delta[CO_3^{2-}]$ values at ~9 ka. Although *H. elegans* were rare in this interval of 46CDH, CdW estimated from *C. pachyderma* suggests relatively low values that lasted until ~7 ka (Figure 6). These oscillations could reflect a brief reduction in the fraction of AAIW relative to northern source waters in response to an abrupt decline in the AMOC, a change in the preformed composition of an endmember, reduced accumulation of respired material in the tropical phosphate maximum, or some combination of these mechanisms. Additional records are needed to confirm this event as well as the Holocene trends, and if confirmed, to distinguish among possible mechanisms.

6 Outstanding Questions

We have interpreted millennial-scale $\Delta[CO_3^{2-}]$ and CdW variations at the Demerara Rise site as evidence of a strong link between deglacial variations in the intensity of AMOC and the influence of relatively low- $\Delta[CO_3^{2-}]$, high-CdW AAIW in the western tropical North Atlantic. In general, when the AMOC is strong, more low–$\Delta[CO_3^{2-}]$, high-CdW AAIW crosses the equator to compensate for the export of NADW (or its glacial equivalent) at depth (e.g., Gu et al., 2017), and the $\Delta[CO_3^{2-}]$ and CdW at the Demerara Rise site decrease and increase respectively. Interpreted in this way, the Demerara Rise $\Delta[CO_3^{2-}]$ and CdW reconstructions are generally consistent with the view based on $^{231}Pa/^{230}Th$ data that the AMOC was modestly strong during the LGM, was weaker during most of HS1, strengthened at the beginning of the BA, was weak again during the YD, and recovered at the end of the YD (McManus et al., 1994, Ng et al., 2018). However, there are departures from this simple model and questions remain about the mechanisms of nutrient and $\Delta[CO_3^{2-}]$ variability, and the role of AMOC in driving deglacial BWT variability in the tropical Atlantic at AAIW depths.

6.1 Timing of deglacial increase of AAIW in the northern subtropics

For example, increasing CdW at several sites (Poggemann et al., 2017; Valley et al., 2017), including the Demerara Rise, and decreasing $\Delta[CO_3^{2-}]$ at the Demerara Rise may imply that the presence of AAIW in the tropical North Atlantic increased before the end of HS1, possibly as early as 17 ka, but more notably at 16 ka. Although one explanation for this increase is a greater northward extent of AAIW due to reinvigoration of the upper AMOC cell, this mechanism implies decoupling between the upper and lower AMOC cells (Valley et al., 2017). Moreover, CdW did not increase at the Brazil Margin site, within AAIW, until ~14.5 ka, implying that this was when AAIW expanded into the South Atlantic (Umling et al., 2019; Yu et al., 2022). The apparent delay between AAIW expansion into the tropics (~16 ka) and into the South Atlantic (~14.5 ka) suggests decoupling between the fraction of AAIW in the South Atlantic and its northward extent in the tropical Atlantic. While model simulations suggest that on the millennial times scale, the northern extent of the AAIW is closely related to the overall AMOC intensity, they also suggest that the AAIW formation rate, and its circulation in the South Atlantic, may be decoupled from its northward extent in the Atlantic (Gu et al., 2017), perhaps reconciling the different timing of the CdW increase on the Brazil Margin and Demerara Rise. On the other hand, given evidence that the overall AMOC was in a weak state until the end of HS1 (e.g., Ng et al., 2018), continued accumulation of respired nutrients cannot be ruled out.

Although the BWT records might help distinguish between these hypotheses, the Florida Margin and Demerara Rise sites have different signals in late HS1. The absence of a clear warming signal at the Florida Margin during late HS1 may be consistent with an increase in AAIW and a reinvigoration of the upper AMOC. On the other hand, the Demerara Rise site continued to warm during late HS1, consistent with a weak AMOC and continued accumulation of respired material. And, as the Brazil Margin reconstruction indicates that AAIW warmed in late HS1 (Figure 6b), AAIW could have contributed to late HS1 tropical warming, as suggested by Poggemann et al. (2018). Clearly additional BWT reconstructions are needed to better constrain tropical warming at AAIW depths and to further evaluate these mechanisms.

6.2 AMOC weakening during the Allerød?

As discussed in Section 5.2, many lines of evidence suggest a significant reinvigoration of the AMOC at the BA onset, including cooling at both the Demerara Rise and Florida Margin sites, a diminished $\Delta[CO_3^{2-}]$ gradient between the Demerara Rise and the Brazil Margin sites, an abrupt increase in CdW at the Brazil Margin (Figure 6), and Demerara Rise neodymium isotope records (Huang et al., 2014).

However, as noted in Section 5.1, the driver of warming at the Demerara Rise and Florida Margin during the Allerød (from the peak of the Bølling to the beginning of the YD) is unclear. One possibility is that this warming was due to a weakening AMOC resulting from orographic effects of a melting ice sheet (Umling et al., 2019; Zhu et al., 2014). The CdW estimated from both *C. pachyderma* and *H. elegans* suggest that CdW began to decrease to YD values soon after the peak of the Bølling, consistent with AMOC weakening. However, the $\Delta[CO_3^{2-}]$ increase, estimated from *C. pachyderma* (thus registered on the exact same samples), does not increase until the beginning of the YD, suggesting decoupling between the two, most likely at the northern source. Regardless, additional data are needed to assess whether a post-Bølling AMOC decrease contributed to deglacial warming in the tropical Atlantic, and if not, to explore other reasons for Allerød warming.

7 Summary

Our new BWT reconstruction from the Demerara Rise confirms that the western tropical Atlantic at AAIW depths warmed during HS1 independent of large local vertical displacement of isopycnals as occurs at the Florida Margin in association with AMOC variability (Lynch-Stieglitz et al., 2014; Valley et al., 2017). Early deglacial warming was likely due to rising greenhouse gases and a weakening AMOC. Warming in AAIW may have contributed to warming at these sites late in HS1 (Poggemann et al., 2018). Both the Florida Margin and Demerara Rise were colder early in the BA (during the Bølling) than they were during the peak warmth of HS1 (Figures 5c and 6b), consistent with reinvigoration of the AMOC (e. g., Pedro et al., 2018).

Although the Demerara Rise site was relatively warm during the YD, warmth appears to have been the culmination of a warming trend during the Allerød, rather than specifically associated with the YD. Greater warming at the Florida Margin than at the Demerara Rise may have been due to isopycnal adjustment associated with reduced geostrophic flow (Valley et al., 2019). Additional BWT reconstructions from the Atlantic at AAIW depths are needed to assess the extent of regional BWT change during the YD.

Our new B/Ca record provides the first clear evidence that $\Delta[CO_3^{2-}]$ in the tropical Atlantic at AAIW depths was tightly coupled to North Atlantic millennial-scale climate variability. We suggest that changes in the contribution of northern and southern sourced waters, in response to AMOC variability, were the main driver of the well-defined millennial $\Delta[CO_3^{2-}]$ variations – with relatively high $\Delta[CO_3^{2-}]$ values during the LGM, early HS1, and the YD indicating greater ventilation by northern sources, and lower values during the BA and after the YD indicating an increased fraction of AAIW and a stronger AMOC. CdW reconstructions are generally consistent with these inferences. The post–YD trend of increasing AAIW/stronger AMOC may have extended to ~ 5 ka, with a superimposed millennial oscillation, but additional data are needed to confirm these inferences.

Our B/Ca and Li/Ca records indicate that at the Demerara Rise site, changes in bottom water $\Delta[CO_3^{2-}]$ are reflected in the micro-environment (calcifying pool) of all three species of benthic foraminifera, including an infaunal species (*Uvigerina peregrina*). This finding suggests that published BWT records based on Mg/Ca of benthic foraminifera should be carefully evaluated. Specifically, our finding of relatively high $\Delta[CO_3^{2-}]$ at ~ 1000 m in the tropical North Atlantic during both HS1 and the YD has implications for BWT estimates based on the Mg/Ca of the calcitic foraminifera. For example, inferred warming during HS1 in the subpolar North Atlantic at ~ 1300 m is based on the Mg/Ca of calcitic benthic foraminifera, especially *Cibicidoides* species (Marcott et al., 2011). However, our new data adds to evidence that the Mg/Ca of *Cibicidoides* species is strongly influenced by $\Delta[CO_3^{2-}]$ (Yu & Elderfield, 2008). Similarly, a Mg/Ca record of the calcitic foraminifera *Globobulimina* in a core from ~ 1300 m in the eastern equatorial Atlantic suggests temperatures and amplitude of BWT variability during the deglaciation (Weldeab et al., 2016a) that are similar to those at the Florida Margin site (not shown). Although the Mg/Ca of this infaunal genus appears to have a high sensitivity to BWT, making it less sensitive to changes in $\Delta[CO_3^{2-}]$ (e.g., Weldeab et al., 2016b), evidence of temperatures at 1300 m as warm as the ~ 550 m at the Florida Margin site during HS1 and the YD should be confirmed. We do not rule out warming during HS1 and the YD at these sites, but suggest that the BWT reconstructions may be influenced by $\Delta[CO_3^{2-}]$ variations across these events and should be replicated using other methods. Mg/Li of *U. peregrina* might be useful at sites where *H. elegans* are absent or scarce.

Acknowledgments

We thank WHOI Seafloor Samples Repository for curating the samples, and WHOI NOSAMS for radiocarbon analyses. We thank K. Pietro, G. Swarr, P.-Y. Lin, A.-L. Chen, and H.-Y. Chen for technical assistance, and two anonymous reviewers for helpful comments. This work was funded by NSF (OCE-2114579, OCE-1811305, OCE-1558341, AGS-0936472, OCE-0750880), Taiwan NSC Postdoctoral Fellowship (NSC 98-2917-I-564-132), Taiwan MOST (104-2628-M-001-007-MY3 and 110-2116-M-001-013), a WHOI Independent Research and Development Award and the Investment in Science Fund at WHOI.

Open Research

Published data used in this study are available in Bryan & Marchitto (2008, 2010), Huang et al. (2014), Lacerra et al. (2019), Marchitto et al. (2018), Oppo et al. (2018), Umling et al. (2019), and Valley et al. (2017, 2019, 2022). Data generated for this study are available in Oppo et al. (2023a). Data and R scripts to reproduce Figs. 5 and 6 are available in Oppo et al. (2023b). Inter-laboratory calibration data are available in the Supporting Information.

References

Bainbridge, A. E. (1981, February 14). GEOSECS Atlantic Expedition Vol. 1 Hydrographic Data, U. S. Government Printing Office, Washington D. C. NSF. Retrieved from http://epic.awi.de/34900/1/atlantic-expedition_vol1.pdf

Barker, S., Kiefer, T., & Elderfield, H. (2004). Temporal changes in North Atlantic circulation constrained by planktonic foraminiferal shell weights. *Paleoceanography*, *19*(3), 1–16. https://doi.org/10.1029/2004PA001004

Barnola, J. M., Raynaud, D., Korotkevich, Y. S., & Lorius, C. (1987). Vostok ice core provides 160,000-year record of atmospheric CO_2. *Nature*, *329*(6138), 408–414. https://doi.org/10.1038/329408a0

Bentov, S., Brownlee, C., & Erez, J. (2009). The role of seawater endocytosis in the biomineralization process in calcareous foraminifera. *Proceedings of the National Academy of Sciences of the United States of America*, *106*(51), 21500–21504. https://doi.org/10.1073/pnas.0906636106

Bentov, S., & Erez, J. (2006). Impact of biomineralization processes on the Mg content of foraminiferal shells: A biological perspective. *Geochemistry, Geophysics, Geosystems*, *7*(1).

https://doi.org/10.1029/2005GC001015

Bereiter, B., Eggleston, S., Schmitt, J., Nehrbass-Ahles, C., Stocker, T. F., Fischer, H., … Chappellaz, J. (2015). Revision of the EPICA Dome C CO2 record from 800 to 600-kyr before present. *Geophysical Research Letters*, *42*(2), 542–549. https://doi.org/10.1002/2014GL061957

Bertram, C. J., Elderfield, H., Shackleton, N. J., & MacDonald, J. A. (1995). Cadmium/calcium and carbon isotope reconstructions of the glacial northeast Atlantic Ocean. *Paleoceanography*, *10*(3), 563–578. https://doi.org/10.1029/94PA03058

Blaauw, M., & Christeny, J. A. (2011). Flexible paleoclimate age-depth models using an autoregressive gamma process. *Bayesian Analysis*, *6*(3), 457–474. https://doi.org/10.1214/11-BA618.

Bond, G. C., W. S. Broecker, S. Johnsen, J. F. McManus, L. Labeyrie, J. Jouzel, & G. Bonani (1993). Correlations between climate records from North Atlantic sediments and Greenland ice. *Nature*, *365*, 143–147.

Boyle, E. A. (1992). Cadmium and $\delta^{13}C$ paleochemical distributions durng the stage 2 glacial maximum. *Annual Reviews Planetary Science*, *20*, 245–287.

Boyle, E.A., & Keigwin, L. D. (1985). Comparison of Atlantic and Pacific paleochemical records for the last 215,000 years: changes in deep ocean circulation and chemical inventories. *Earth and Planetary Science Letters*, *76*(1–2), 135–150. https://doi.org/10.1016/0012-821X(85)90154-2

Boyle, E. A. (1988). Cadmium: Chemical tracer of deepwater paleoceanography. *Paleoceanography*, *3*(4), 471–489. https://doi.org/10.1029/PA003i004p00471

Boyle, E. A., Labeyrie, L., & Duplessly, J.-C. (1995). Calcitic foraminiferal data confirmed by cadmium in aragonitic *Hoeglundina* : Application to the Last Glacial Maximum in the northern Indian Ocean. *Paleoceanography*, *10*(5), 881–900. https://doi.org/10.1029/95PA01625

Boyle, E., & Rosenthal, Y. (1996). Chemical Hydrography of the South Atlantic During the Last Glacial Maximum: Cd vs. $d^{13}C$. In G. Wefer, W. H. Berger, G. Siedler, D. J. Webb (eds.) *The South Atlantic: Present and Past Circulation* (pp. 423-443). Heidelberg, Germany: Springer-Verlag Berlin.

Bryan, S P, & Marchitto, T. M. (2010). Testing the utility of paleonutrient proxies Cd/Ca and Zn/Ca in benthic foraminifera from thermocline waters. *Geochemistry Geophysics Geosystems*, *11*, Q01005. https://doi.org/10.1029/2009gc002780

Bryan, S. P., & Marchitto, T. M. (2008). Mg/Ca-temperature proxy in benthic foraminifera: New calibrations from the Florida Straits and a hypothesis regarding Mg/Li. *Paleoceanography*, *23*(2), 1–17. https://doi.org/10.1029/2007PA001553

Came, R. E., Oppo, D. W., Curry, W. B., & Lynch-Stieglitz, J. (2008). Deglacial variability in the surface return flow of the Atlantic meridional overturning circulation. *Paleoceanography*, *23*(1). https://doi.org/10.1029/2007PA001450

Corliss, B. H. (1991). Morphology and microhabitat preferences of benthic foraminifera from the northwest Atlantic Ocean. *Marine Micropaleontology*, *17*(3–4), 195–236. https://doi.org/10.1016/0377-8398(91)90014-W

Dahl, K. A., Broccoli, A. J., & Stouffer, R. J. (2005). Assessing the role of North Atlantic freshwater forcing in millennial scale climate variability: A tropical Atlantic perspective. *Climate Dynamics*, *24*(4), 325–346. https://doi.org/10.1007/s00382-004-0499-5

de Nooijer, L. J., Toyofuku, T., & Kitazato, H. (2009). Foraminifera promote calcification by elevating their intracellular pH. *Proceedings of the National Academy of Sciences of the United States of America*, *106*(36), 15374–15378. https://doi.org/10.1073/pnas.0904306106

Doss, W., Marchitto, T. M., Eagle, R., Rashid, H., & Tripati, A. (2018). Deconvolving the saturation state and temperature controls on benthic foraminiferal Li/Ca, based on downcore paired B/Ca measurements and coretop compilation. *Geochimica et Cosmochimica Acta*. https://doi.org/10.1016/j.gca.2018.02.029

Duteil, O., Koeve, W., Oschlies, A., Aumont, O., Bianchi, D., Bopp, L., … Segschneider, J. (2012). Preformed and regenerated phosphate in ocean general circulation models: can right total concentrations be wrong? *Biogeosciences*, *9*(5), 1797–1807. https://doi.org/10.5194/bg-9-1797-2012

Elderfield, H. (1996). A biomineralization model for the incorporation of trace elements into foraminiferal calcium carbonate. *Earth and Planetary Science Letters*, *142*(3–4), 409–423. https://doi.org/10.1016/0012-821X(96)00105-7

Elderfield, H., Greaves, M., Barker, S., Hall, I. R., Tripati, A., Ferretti, P., … Daunt, C. (2010). A record of bottom water temperature and seawater δ18O for the Southern Ocean over the past 440kyr based on Mg/Ca of benthic foraminiferal Uvigerina spp. *Quaternary Science Reviews*, *29*(1), 160–169. https://doi.org/10.1016/j.quascirev.2009.07.013

Elderfield, H., Yu, J., Anand, P., Kiefer, T., & Nyland, B. (2006). Calibrations for benthic foraminiferal Mg/Ca paleothermometry and the carbonate ion hypothesis. *Earth and Planetary Science Letters*, *250*(3–4), 633–649. https://doi.org/10.1016/j.epsl.2006.07.041

Erez, J. (2003). The Source of Ions for Biomineralization in Foraminifera and Their Implications for Paleoceanographic Proxies. *Rev. Mineral. Geochem.*, *54*, 115–149.

Fontanier, C., MacKensen, A., Jorissen, F. J., Anschutz, P., Licari, L., & Griveaud, C. (2006). Stable oxygen and carbon isotopes of live benthic foraminifera from the Bay of Biscay: Microhabitat impact and seasonal variability. *Marine Micropaleontology*, *58*(3), 159–183. https://doi.org/10.1016/j.marmicro.2005.09.004

Gaetani, G. A., & Cohen, A. L. (2006). Element partitioning during precipitation of aragonite from seawater: A framework for understanding paleoproxies. *Geochimica et Cosmochimica Acta*, *70*(18), 4617–4634. https://doi.org/10.1016/j.gca.2006.07.008

Garcia, H. E., Weathers, W., Paver, C. R., Smolyar, I., Boyer, T. P. Locarnini, R. A., Zweng, M. M., Mishonov, A. V., Baranova, O. K.. Seidov, D. & Reagan, J. R. (2018). World Ocean Atlas 2018, Volume 4: Dissolved Inorganic Nutrients. A. Mishonov Technical Ed.; NOAA Atlas NESDIS 84, 35pp.

Gebbie, G. (2014). How much did Glacial North Atlantic Water shoal? *Paleoceanography*, *29*(3), 190–209. https://doi.org/10.1002/2013PA002557

Gu, S., Liu, Z., Zhang, J., Rempfer, J., Joos, F., & Oppo, D. W. (2017). Coherent Response of Antarctic Intermediate Water and Atlantic Meridional Overturning Circulation During the Last Deglaciation: Reconciling Contrasting Neodymium Isotope Reconstructions From the Tropical Atlantic. *Paleoceanography*, *32*(10). https://doi.org/10.1002/2017PA003092

Gu, S., Liu, Z., Oppo, D. W., Lynch-Stieglitz, J., Jahn, A., Zhang, J., … Wu, L. (2021). Remineralization dominating the $\delta^{13}C$ decrease in the mid-depth Atlantic during the last deglaciation. *Earth and Planetary Science Letters*, *571*, 117106. https://doi.org/10.1016/j.epsl.2021.117106

Hall, J. M., & Chan, L. H. (2004). Li/Ca in multiple species of benthic and planktonic foraminifera: Thermocline, latitudinal, and glacial-interglacial variation. *Geochimica et Cosmochimica Acta*, *68*(3), 529–545. https://doi.org/10.1016/S0016-7037(00)00451-4

He, C., Liu, Z., Zhu, J., Zhang, J., Gu, S., Otto-Bliesner, B. L., … Sun, J. (2020). North Atlantic subsurface temperature response controlled by effective freshwater input in "Heinrich" events. *Earth and Planetary Science Letters*, *539*, 116247. https://doi.org/10.1016/j.epsl.2020.116247

Heaton, T. J., Köhler, P., Butzin, M., Bard, E., Reimer, R. W., Austin, W. E. N., … Skinner, L. C. (2020). Marine20 - The Marine Radiocarbon Age Calibration Curve (0-55,000 cal BP). *Radiocarbon*, *62*(4), 779–820. https://doi.org/10.1017/RDC.2020.68

Hines, S. K. V., Eiler, J. M., Southon, J. R., & Adkins, J. F. (2019). Dynamic Intermediate Waters Across the Late Glacial Revealed by Paired Radiocarbon and Clumped Isotope Temperature Records. *Paleoceanography and Paleoclimatology*, *34*(7), 1074–1091. https://doi.org/10.1029/2019PA003568

Huang, K.-F., Oppo, D. W., & Curry, W. B. (2014). Decreased influence of Antarctic intermediate water in the tropical Atlantic during North Atlantic cold events. *Earth and Planetary Science Letters*, *389*. https://doi.org/10.1016/j.epsl.2013.12.037

Huang, K.-F., You, C.-F., Lin, H.-L., & Shieh, Y.-T. (2008). In situ calibration of Mg/Ca ratio in planktonic foraminiferal shell using time series sediment trap: A case study of intense dissolution artifact in the South China Sea. *Geochemistry, Geophysics, Geosystems*, *9*(4), Q04016. https://doi.org/10.1029/2007GC001660

Key, R.M., Olsen, van Heuven, S., Lauvset, S. K., Velo, A., Lin, X., Schirnick, C., Kozyr, A.,Tanhua, T., Hoppema, M., Jutterström, S., Steinfeldt, R., Jeansson, E. Ishii, M., Pérez, F. F. & Suzuki, T. (2015). Global Ocean Data Analysis Project, Version 2 (GLODAPv2), ORNL/CDIAC-162, NDP-093. Carbon Dioxide Information Analysis Center, Oak Ridge National Laboratory, US Department of Energy, Oak Ridge, Tennessee. doi:10.3334/CDIAC/OTG.NDP093_GLODAPv2

Kindler, P., Guillevic, M., Baumgartner, M., Schwander, J., Landais, A., & Leuenberger, M. (2014). Temperature reconstruction from 10 to 120 kyr b2k from the NGRIP ice core. *Climate of the Past*, *10*(2), 887–902. https://doi.org/10.5194/cp-10-887-2014

Kroopnick, P. M. (1985). The distribution of 13C of ΣCO2 in the world oceans. *Deep Sea Research Part A. Oceanographic Research Papers*, *32*(1), 57–84. https://doi.org/10.1016/0198-0149(85)90017-2

Lacerra, M., Lund, D. C., Gebbie, G., Oppo, D. W., Yu, J., Schmittner, A., & Umling, N. E. (2019). Less Remineralized Carbon in the Intermediate-Depth South Atlantic During Heinrich Stadial 1. *Paleoceanography and Paleoclimatology*, *34*(7). https://doi.org/10.1029/2018PA003537

Lear, C. H., & Rosenthal, Y. (2006). Benthic foraminiferal Li/Ca: Insights into Cenozoic seawater carbonate saturation state. *Geology*, *34*(11), 985–988. https://doi.org/10.1130/G22792A.1

Lear, C. H., Rosenthal, Y., & Slowey, N. (2002). Benthic foraminiferal Mg/Ca-paleothermometry: A revised core-top calibration. *Geochimica et Cosmochimica Acta*, *66*(19), 3375–3387. https://doi.org/10.1016/S0016-7037(02)00941-9

Lewis, E. R., & Wallace, D. W. R. (1998) *Program Developed for CO2 System Calculations*. United States. https://doi.org/10.15485/1464255

Liu, Z., Otto-Bliesner, B. L., He, F., Brady, E. C., Tomas, R., Clark, P. U., … Cheng, J. (2009). Transient simulation of last deglaciation with a new mechanism for Bolling-Allerod warming. *Science*, *325*(5938), 310–314. https://doi.org/10.1126/science.1171041

Locarnini, R. A., Mishonov, A. V., Baranova, O. K., Boyer, T. P., Zweng, M. M., Garcia, H. E., Reagan, J. R., Seidov, D., Weathers, K., Paver, C. R. & Smolyar, I. (2018). World Ocean Atlas 2018, Volume 1: Temperature. A. Mishonov Technical Ed.; NOAA Atlas NESDIS

81, 52pp.

Lund, D. C., Tessin, A. C., Hoffman, J. L., & Schmittner, A. (2015). Southwest Atlantic water mass evolution during the last deglaciation, 477–494. https://doi.org/10.1002/2014PA002657.Received

Lynch-Stieglitz, J., Schmidt, M. W., Gene Henry, L., Curry, W. B., Skinner, L. C., Mulitza, S., … Chang, P. (2014). Muted change in Atlantic overturning circulation over some glacial-aged Heinrich events. *Nature Geoscience*, *7*(2), 144–150. https://doi.org/10.1038/ngeo2045

Lynch-Stieglitz, J., Valley, S. G., & Schmidt, M. W. (2019). Temperature-dependent ocean–atmosphere equilibration of carbon isotopes in surface and intermediate waters over the deglaciation. *Earth and Planetary Science Letters*, *506*, 466–475. https://doi.org/10.1016/j.epsl.2018.11.024

Marchitto Jr., T. M., Curry, W. B., & Oppo, D. W. (2000). Zinc concentrations in benthic foraminifera reflect seawater chemistry. *Paleoceanography*, *15*(3). https://doi.org/10.1029/1999PA000420

Marchitto, T. M., Bryan, S. P., Doss, W., McCulloch, M. T., & Montagna, P. (2018). A simple biomineralization model to explain Li, Mg, and Sr incorporation into aragonitic foraminifera and corals. *Earth and Planetary Science Letters*, *481*, 20–29. https://doi.org/10.1016/j.epsl.2017.10.022

Marchitto, Thomas M. (2006). Precise multielemental ratios in small foraminiferal samples determined by sector field ICP-MS. *Geochemistry, Geophysics, Geosystems*, *7*(5), Q05P13. https://doi.org/10.1029/2005GC001018

Marchitto, T. M., & Broecker, W. S. (2006). Deep water mass geometry in the glacial Atlantic Ocean: A review of constraints from the paleonutrient proxy Cd/Ca. *Geochemistry, Geophysics, Geosystems*, *7*(12). https://doi.org/10.1029/2006GC001323

Marcott, S. A., Clark, P. U., Padman, L., Klinkhammer, G. P., Springer, S. R., Liu, Z., … Schmittner, A. (2011). Ice-shelf collapse from subsurface warming as a trigger for Heinrich events. *Proceedings of the National Academy of Sciences of the United States of America*, *108*(33), 13415–13419. https://doi.org/10.1073/pnas.1104772108

Marriott, C. S., Henderson, G. M., Belshaw, N. S., & Tudhope, A. W. (2004). Temperature dependence of δ7Li, δ44Ca and Li/Ca during growth of calcium carbonate. *Earth and Planetary Science Letters*, *222*(2), 615–624. https://doi.org/10.1016/j.epsl.2004.02.031

Martin, P. A., Lea, D. W., Rosenthal, Y., Shackleton, N. J., Sarnthein, M., & Papenfuss, T. (2002). Quaternary deep sea temperature histories derived from benthic foraminiferal Mg/Ca. *Earth and Planetary Science Letters*, *198*(1–2), 193–209. https://doi.org/10.1016/S0012-821X(02)00472-7

Max, L., Nürnberg, D., Chiessi, C. M., Lenz, M. M., & Mulitza, S. (2022). Subsurface ocean warming preceded Heinrich Events. *Nature Communications*, *13*(1), 4217. https://doi.org/10.1038/s41467-022-31754-x

McCorkle, D. C., Martin, P. A., Lea, D. W., & Klinkhammer, G. P. (1995). Evidence of a dissolution effect on benthic foraminiferal shell chemistry: δ ^{13} C, Cd/Ca, Ba/Ca, and Sr/Ca results from the Ontong Java Plateau. *Paleoceanography*, *10*(4), 699–714. https://doi.org/10.1029/95PA01427

McKay, N. P., Emile-Geay, J., & Khider, D. (2021). geoChronR – an R package to model, analyze, and visualize age-uncertain data. *Geochronology*, *3*(1), 149–169. https://doi.org/10.5194/gchron-3-149-2021

McManus, J. F., Francois, R., Gherardi, J.-M., Keigwin, L. D., & Brown-Leger, S. (2004).

Collapse and rapid resumption of Atlantic meridional circulation linked to deglacial climate changes. *Nature*, *428*(6985), 834–837. https://doi.org/10.1038/nature02494

Menviel, L., Spence, P., & England, M. H. (2015). Contribution of enhanced Antarctic Bottom Water formation to Antarctic warm events and millennial-scale atmospheric CO2 increase. *Earth and Planetary Science Letters*, *413*, 37–50. https://doi.org/10.1016/j.epsl.2014.12.050

Middag, R., van Heuven, S. M. A. C., Bruland, K. W., & de Baar, H. J. W. (2018). The relationship between cadmium and phosphate in the Atlantic Ocean unravelled. *Earth and Planetary Science Letters*, *492*, 79–88. https://doi.org/10.1016/j.epsl.2018.03.046

Ng, H. C., Robinson, L. F., McManus, J. F., Mohamed, K. J., Jacobel, A. W., Ivanovic, R. F., … Chen, T. (2018). Coherent deglacial changes in western Atlantic Ocean circulation. *Nature Communications*, *9*(1), 2947. https://doi.org/10.1038/s41467-018-05312-3

Nürnberg, D., Bijma, J., & Hemleben, C. (1996). Assessing the reliability of magnesium in foraminiferal calcite as a proxy for water mass temperatures. *Geochimica et Cosmochimica Acta*, *60*(5), 803–814. https://doi.org/10.1016/0016-7037(95)00446-7

Olsen, A., Key, R. M., van Heuven, S., Lauvset, S. K., Velo, A., Lin, X., Schirnick, C., Kozyr, A., Tanhua, T., Hoppema, M., Jutterström, S., Steinfeldt, R., Jeansson, E., Ishii, M., Pérez, F. F. & Suzuki, T. (2016) The Global Ocean Data Analysis Project version 2 (GLODAPv2) – an internally consistent data product for the world ocean, *Earth Syst. Sci. Data*, 8, 297–323. doi:10.5194/essd-8-297-2016

Oomori, T., Kaneshima, H., Maezato, Y., & Kitano, Y. (1987). Distribution coefficient of Mg2+ ions between calcite and solution at 10-50°C. *Marine Chemistry*, *20*(4), 327–336. https://doi.org/10.1016/0304-4203(87)90066-1

Oppo, D. W., Gebbie, G., Huang, K.-F., Curry, W. B., Marchitto, T. M., & Pietro, K. R. (2018). Data Constraints on Glacial Atlantic Water Mass Geometry and Properties. *Paleoceanography and Paleoclimatology*, *33*(9). https://doi.org/10.1029/2018PA003408

Oppo, D. W., Lu, W., Huang, K-F., Umling, N. E., Guo, W., Yu, J., Curry, W. B., Marchitto, T. M., & Wang, S. (2023a). Demerara Rise d13C, d18O, Trace Metal and Reconstructed Bottom Water Temperature Data Over the Past 20 ka. [Dataset]. NOAA National Centers for Environmental Information. https://doi.org/10.25921/71sa-8v70

Oppo, D. W., Lu, W., Huang, K.-F., Umling, N. E., Guo, W., Yu, J., Curry, W. B., Marchitto, T. M., & Wang, S. (2023b). Deglacial temperature and carbonate saturation state variability in the tropical Atlantic at Antarctic Intermediate Water depths [Dataset]. *Zenodo*. https://doi.org/10.5281/zenodo.8229878

Pedro, J. B., Jochum, M., Buizert, C., He, F., Barker, S., & Rasmussen, S. O. (2018). Beyond the bipolar seesaw: Toward a process understanding of interhemispheric coupling. *Quaternary Science Reviews*, *192*, 27–46. https://doi.org/10.1016/j.quascirev.2018.05.005

Poggemann, D.-W., Hathorne, E. C., Nürnberg, D., Frank, M., Bruhn, I., Reißig, S., & Bahr, A. (2017). Rapid deglacial injection of nutrients into the tropical Atlantic via Antarctic Intermediate Water. *Earth and Planetary Science Letters*, *463*, 118–126. https://doi.org/10.1016/j.epsl.2017.01.030

Poggemann, D. W., Nürnberg, D., Hathorne, E. C., Frank, M., Rath, W., Reißig, S., & Bahr, A. (2018). Deglacial Heat Uptake by the Southern Ocean and Rapid Northward Redistribution Via Antarctic Intermediate Water. *Paleoceanography and Paleoclimatology*, *33*(11), 1292–1305. https://doi.org/10.1029/2017PA003284

Rae, J. W. B., Foster, G. L., Schmidt, D. N., & Elliott, T. (2011). Boron isotopes and B/Ca in benthic foraminifera: Proxies for the deep ocean carbonate system. *Earth and Planetary*

Science Letters, *302*(3–4), 403–413. https://doi.org/10.1016/j.epsl.2010.12.034

Rafter, P. A., Gray, W. R., Hines, S. K. V., Burke, A., Costa, K. M., Gottschalk, J., … DeVries, T. (2022). Global reorganization of deep-sea circulation and carbon storage after the last ice age. *Science Advances*, *8*(46), 1–10. https://doi.org/10.1126/sciadv.abq5434

Rosenthal, Y., Lear, C. H., Oppo, D. W., & Linsley, B. K. (2006). Temperature and carbonate ion effects on Mg/Ca and Sr/Ca ratios in benthic foraminifera: Aragonitic species Hoeglundina elegans. *Paleoceanography*, *21*(1). https://doi.org/10.1029/2005PA001158

Rosenthal, Yair, Field, M. P., & Sherrell, R. M. (1999). Precise Determination of Element / Calcium Ratios in Calcareous Samples Using Sector Field Inductively Coupled Plasma Mass Spectrometry. *Analytical Chemistry*, *71*(15), 3248–3253.

Sarmiento, J. L., Gruber, N., Brzezinski, M. A., & Dunne, J. P. (2004). High-latitude controls of thermocline nutrients and low latitude biological productivity. *Nature*, *427*(6969), 56–60. https://doi.org/10.1038/nature02127

Schlitzer, R. (2015). Ocean Data View. Available on https://odv.awi.de/ (2015).

Schmidt, M. W., Chang, P., Hertzberg, J. E., Them, T. R., Ji, L., J, L., & Otto-Bliesner, B. L. (2012). Impact of abrupt deglacial climate change on tropical Atlantic subsurface temperatures. *Proceedings of the National Academy of Sciences of the United States of America*, *109*(36), 14348–14352. https://doi.org/10.1073/pnas.1207806109

Schmittner, A., & Lund, D. C. (2015). Early deglacial Atlantic overturning decline and its role in atmospheric CO_2 rise inferred from carbon isotopes ($\delta^{13}C$). *Climate of the Past*, *11*(2), 135–152. https://doi.org/10.5194/cp-11-135-2015

Seierstad, I. K., Abbott, P. M., Bigler, M., Blunier, T., Bourne, A. J., Brook, E., … Vinther, B. M. (2014). Consistently dated records from the Greenland GRIP, GISP2 and NGRIP ice cores for the past 104ka reveal regional millennial-scale δ18O gradients with possible Heinrich event imprint. *Quaternary Science Reviews*, *106*, 29–46. https://doi.org/10.1016/j.quascirev.2014.10.032

Szuts, Z. B., & Meinen, C. S. (2017). Florida Current Salinity and Salinity Transport: Mean and Decadal Changes. *Geophysical Research Letters*, *44*(20), 10,495-10,503. https://doi.org/10.1002/2017GL074538

Thiagarajan, N., Subhas, A. V, Southon, J. R., Eiler, J. M., & Adkins, J. F. (2014). Abrupt pre-Bolling-Allerod warming and circulation changes in the deep ocean. *Nature*, *511*(7507), 75–78. https://doi.org/10.1038/nature13472

Tuerena, R. E., Ganeshram, R. S., Geibert, W., Fallick, A. E., Dougans, J., Tait, A., … Woodward, E. M. S. (2015). Global Biogeochemical Cycles, 1830–1844. https://doi.org/10.1002/2015GB005164.Received

Umling, N. E., Oppo, D. W., Chen, P., Yu, J., Liu, Z., Yan, M., … Toledo, F. A. L. (2019). Atlantic Circulation and Ice Sheet Influences on Upper South Atlantic Temperatures During the Last Deglaciation. *Paleoceanography and Paleoclimatology*, *34*(6). https://doi.org/10.1029/2019PA003558

Valley, S. G., Lynch-Stieglitz, J., & Marchitto, T. M. (2019). Intermediate water circulation changes in the Florida Straits from a 35 ka record of Mg/Li-derived temperature and Cd/Ca-derived seawater cadmium. *Earth and Planetary Science Letters*, *523*, 115692. https://doi.org/10.1016/j.epsl.2019.06.032

Valley, S. G., Lynch-Stieglitz, J., Marchitto, T. M., & Oppo, D. W. (2022). Seawater Cadmium in the Florida Straits Over the Holocene and Implications for Upper AMOC Variability. *Paleoceanography and Paleoclimatology*, *37*(5), 1–12.

https://doi.org/10.1029/2021PA004379

Valley, S., Lynch-Stieglitz, J., & Marchitto, T. M. (2017). Timing of Deglacial AMOC Variability From a High-Resolution Seawater Cadmium Reconstruction. *Paleoceanography*, *32*(11), 1195–1203. https://doi.org/10.1002/2017PA003099

Weldeab, S., Arce, A., & Kasten, S. (2016). Mg/Ca-$\Delta\mathrm{CO}_3^{2-}{}_{\text{pore water}}$–temperature calibration for *Globobulimina* spp.: A sensitive paleothermometer for deep-sea temperature reconstruction. *Earth and Planetary Science Letters*, *438*, 95–102. https://doi.org/10.1016/j.epsl.2016.01.009

Weldeab, S., Friedrich, T., Timmermann, A., & Schneider, R. R. (2016). Strong middepth warming and weak radiocarbon imprints in the equatorial Atlantic during Heinrich 1 and Younger Dryas. *Paleoceanography*, *31*(8), 1070–1082. https://doi.org/10.1002/2016PA002957

Xie, R. C., Marcantonio, F., & Schmidt, M. W. (2012). Deglacial variability of Antarctic Intermediate Water penetration into the North Atlantic from authigenic neodymium isotope ratios. *Paleoceanography*, *27*(3), 1–12. https://doi.org/10.1029/2012PA002337

Yu, J., Menviel, L., Jin, Z. D., Thornalley, D. J. R., Foster, G. L., Rohling, E. J., … Roberts, A. P. (2019). More efficient North Atlantic carbon pump during the Last Glacial Maximum. *Nature Communications*, *10*(1), 1–11. https://doi.org/10.1038/s41467-019-10028-z

Yu, J., Broecker, W. S., Elderfield, H., Jin, Z., McManus, J., & Zhang, F. (2010). Loss of carbon from the deep sea since the last glacial maximum. *Science*, *330*(6007), 1084–1087. https://doi.org/10.1126/science.1193221

Yu, J., & Elderfield, H. (2007). Benthic foraminiferal B/Ca ratios reflect deep water carbonate saturation state. *Earth and Planetary Science Letters*, *258*(1–2), 73–86. https://doi.org/10.1016/j.epsl.2007.03.025

Yu, J., & Elderfield, H. (2008). Mg/Ca in the benthic foraminifera Cibicidoides wuellerstorfi and Cibicidoides mundulus: Temperature versus carbonate ion saturation. *Earth and Planetary Science Letters*, *276*(1–2), 129–139. https://doi.org/10.1016/j.epsl.2008.09.015

Yu, J., Elderfield, H., & Piotrowski, A. M. (2008). Seawater carbonate ion-δ^{13}C systematics and application to glacial-interglacial North Atlantic ocean circulation. *Earth and Planetary Science Letters*, *271*(1–4), 209–220. https://doi.org/10.1016/j.epsl.2008.04.010

Yu, J., Oppo, D. W., Jin, Z., Lacerra, M., Ji, X., Umling, N. E., … Xu, C. (2022). Millennial and centennial CO2 release from the Southern Ocean during the last deglaciation. *Nature Geoscience*, *15*(4), 293–299. https://doi.org/10.1038/s41561-022-00910-9

Zhang, J., Liu, Z., Brady, E. C., Jahn, A., Oppo, D. W., Clark, P. U., … Lindsay, K. (2017). Asynchronous warming and oxygen isotope evolution of deep Atlantic water masses during the last deglaication. *Proceedings of the National Academy of Sciences*, 114(42), 11075-11080. https://doi.org/10.1073/pnas.1704512114

Zhu, J., Liu, Z., Zhang, X., Eisenman, I., & Liu, W. (2014). Linear weakening of the AMOC in response to receding glacial ice sheets in CCSM3. *Geophysical Research Letters*, *41*(17), 6252–6258. https://doi.org/10.1002/2014GL060891

Figure Captions.

Figure 1. Location of cores discussed. (a) In red, from south to north, Brazil Margin site KNR159-5-90GGC (e. g., Lacerra et al., 2019; Umling et al., 2019), Demerara Rise site KNR197-3-46CDH (Huang et al., 2014; Oppo et al., 2018; this study), and Florida Strait site KNR166-2-26JPC (e.g., Lynch-Stieglitz et al., 2014; Valley et al., 2017, 2019). Tobago Basin site M78/235-1 is shown in

yellow (Poggemann et al., 2017, 2018). (b-d) Salinity, phosphate, and $\Delta[CO_3^{2-}]$ sections versus latitude along western Atlantic transect (top). In b, the cores of the low and high salinity water masses are labelled as AAIW and NADW, respectively. Hydrographic data are from the World Ocean Circulation Experiment (Garcia et al., 2018; Locarnini et al., 2018) and from GLODAP (Olsen et al., 2018; Key et al., 2018). Carbonate saturation state was calculated with CO2SYS (Lewis & Wallace, 1998). Figure was made in Ocean Data View (Schlitzer, 2015).

Figure 2. Core-top relationships between BWT and Mg/Ca (a-c) and Mg/Li (d-f). Panels a) and d) are for *C. pachyderma*, b) and e) are for *U. peregrina* and c) and f) are for *H. elegans*. Li/Ca versus BWT and Mg/Ca, Li/Ca, and Mg/Li versus saturation state are shown in Figure S6 in Supporting Information SI. *H. elegans* data are corrected for lab offsets as discussed in Supporting Information SI.

Figure 3. Relationship between bottom water temperature (BWT) and core-top *H. elegans* Mg/Li data generated at INSTAAR (red) (Bryan & Marchitto, 2008; Marchitto et al., 2018; Valley et al. 2019; 2022) and WHOI (Demerara Rise in blue, other sites in cyan; this study, Umling et al., 2019) (Data Set S3). Solid black line indicates calibration from Marchitto et al. (2018). Red line shows linear calibration from this study (Mg/Li = 0.1794 + 0.01484 x BWT). Gravity or piston core samples that were not dated or with age > 1 ka (open symbols) were excluded from linear calibration.

Figure 4. Downcore records vs. depth at 46CDH (Data Set S5 in Supporting Information S1). Blue, black, and red correspond to *C. pachyderma, U. peregrina*, and *H. elegans*, respectively. In panel d, BWT reconstructions are based on Mg/Li, except for the record in grey, which is based on the Mg/Ca of *U. peregrina*. For *U. peregrina* and *C. pachyderma*, local calibrations are used. For *H. elegans*, the new linear calibration is used. In panel f, CdW is estimated using distribution coefficients from Boyle (1992) and Boyle et al. (1995). In a and b, axes for *H. elegans* and the calcitic foraminifera are shown on the left and right, respectively. Modern seawater values are shown in d and c. The depths of the LGM and MH (7-6 ka) are shaded.

Figure 5. Records from KNR197-3-46CDH compared to (a) Greenland $\delta^{18}O$ (Seierstad et al., 2014). (b) $\Delta[CO_3^{2-}]$ reconstruction, (c) BWT reconstruction, (e) benthic $\delta^{18}O$, and (e) CdW reconstruction. Reconstructions based on *H. elegans* and *C. pachyderma* are shown in red and blue, respectively. Thick colored lines correspond to the median proxy ensemble member, and ribbons denote 95% highest-density probability ranges as determined by R-package "geoChronR" (McKay et al., 2021). Solid symbols denote sample averages (benthic $\delta^{18}O$) or raw proxy data (others) on their median BACON age. Radiocarbon control and benthic $\delta^{18}O$ tie point are shown in blue and black diamonds, respectively. Shading denotes climate events discussed in text. Heinrich Stadial 1 (HS1) is divided into an early, middle, and late interval. The Bølling is denoted by cyan, and the Allerød by light blue. Solid vertical line denotes the 9-ka event discussed in text. Errors for individual estimates shown are B) ±10μmol/mol (Oppo et al. (2018), c) ±1.4°C, D) average ±0.08‰ (1 standard deviation of replicate $\delta^{18}O$ measurements), and e) ±0.1nmol/kg. Due to uncertain distribution coefficients, the uncertainty for CdW estimates is larger than shown, as discussed in text.

Figure 6. Reconstructions from Demerara Rise core KNR197-3-46CDH (red), Brazil Margin core KNR159-5-90GGC (purple), and Florida Margin core KNR166-2-26JPC (green) compared to North Greenland $\delta^{18}O$ (Seierstad et al., 2014) (a) and atmospheric CO_2 (Beretier et al., 2015) (e). Reconstructions in b) are based on the Mg/Li of *H. elegans* (Umling et al., 2019; Valley et al. 2019; this paper); in c) based on the B/Ca of *C. pachyderma* (Lacerra et al. 2019, and this paper), and in d) on the Cd/Ca of *H. elegans* (Umling et al., 2019; Valley et al. 2017; this paper). For KNR197-3-46CDH , the CdW reconstruction based on Cd/Ca of *C. pachyderma* is also shown in blue. Modern values in b-d are shown as stars on the left. Bold solid lines and shading in b-d are the median proxy ensemble member and 95% highest-density probability ranges, respectively. Individual data points are shown on their median BACON age. Named climate intervals are shaded. The Bølling is denoted by cyan, and the Allerød by light blue.

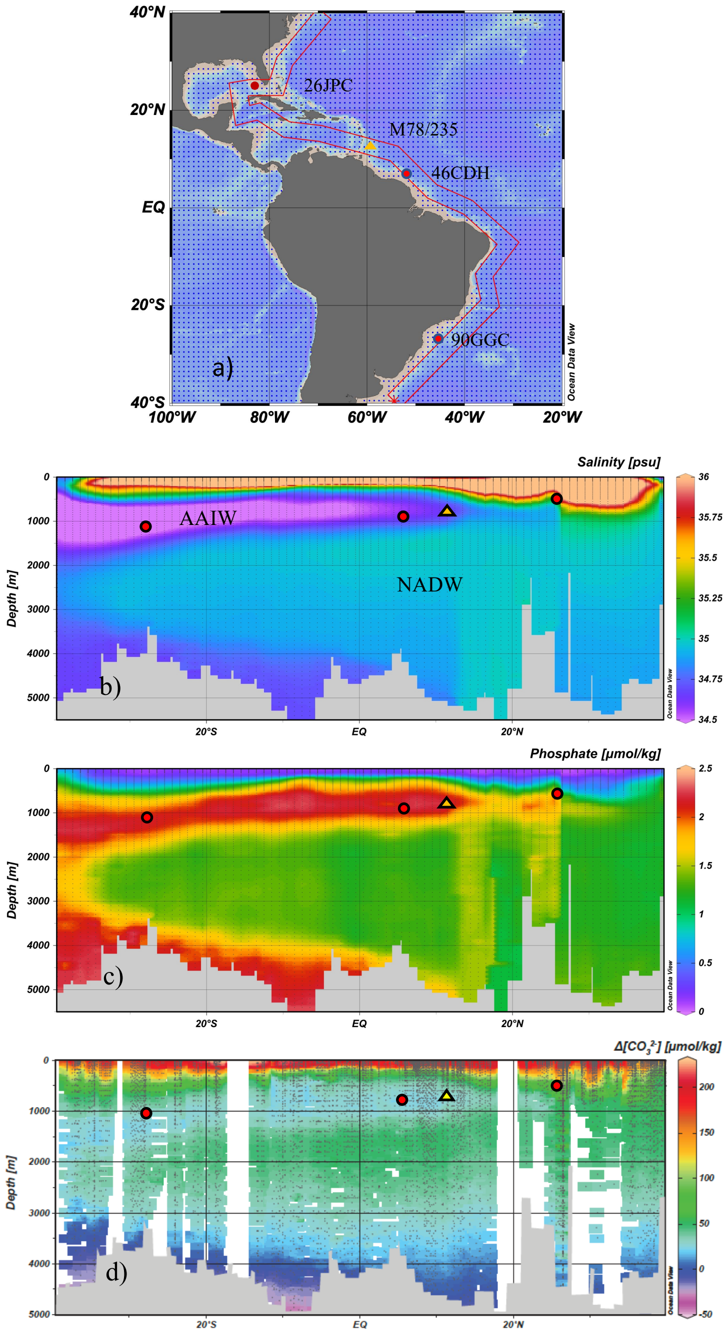
40°N
20°N
EQ
20°S
40°S
100°W
80°W
60°W
40°W
20°W
26JPC
M78/235
46CDH
90GGC
a)
Ocean Data View
Salinity [psu]
AAIW
NADW
b)
Depth [m]
0
1000
2000
3000
4000
5000
20°S
EQ
20°N
36
35.75
35.5
35.25
35
34.75
34.5
Phosphate [µmol/kg]
c)
2.5
2
1.5
1
0.5
0
$\Delta[CO_3^{2-}]$ [µmol/kg]
d)
200
150
100
50
0
-50

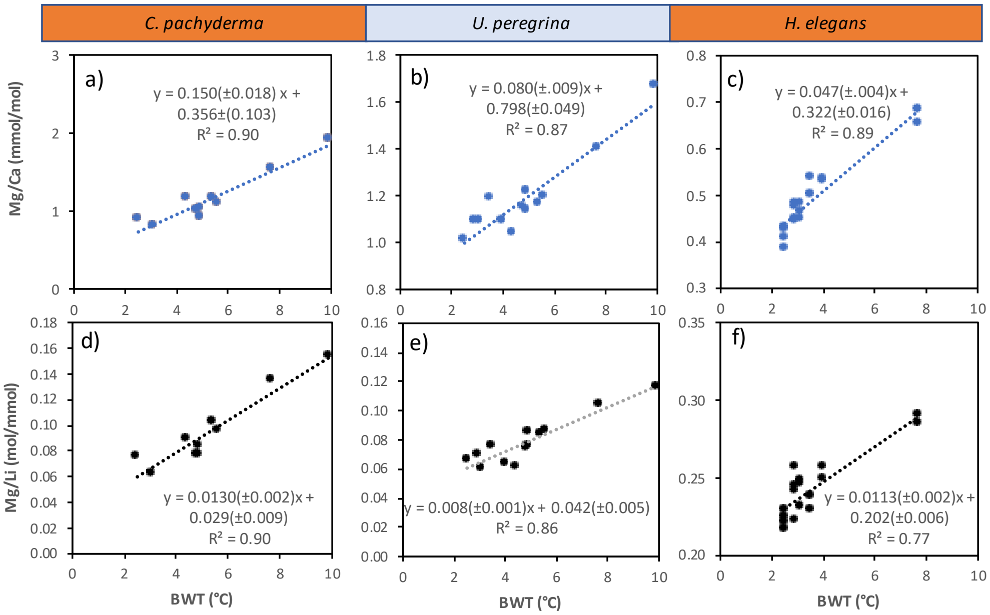
C. pachyderma
U. peregrina
H. elegans
Mg/Ca (mmol/mol)
Mg/Li (mol/mmol)
a)
y = 0.150(±0.018) x + 0.356±(0.103)
R² = 0.90
b)
y = 0.080(±.009)x + 0.798(±0.049)
R² = 0.87
c)
y = 0.047(±.004)x + 0.322(±0.016)
R² = 0.89
d)
y = 0.0130(±0.002)x + 0.029(±0.009)
R² = 0.90
e)
y = 0.008(±0.001)x + 0.042(±0.005)
R² = 0.86
f)
y = 0.0113(±0.002)x + 0.202(±0.006)
R² = 0.77
BWT (°C)
0
2
4
6
8
10
3
2
1
0
1.8
1.6
1.4
1.2
1.0
0.8
0.7
0.6
0.5
0.4
0.3
0.18
0.16
0.14
0.12
0.10
0.08
0.06
0.04
0.02
0.00
0.35
0.30
0.25
0.20

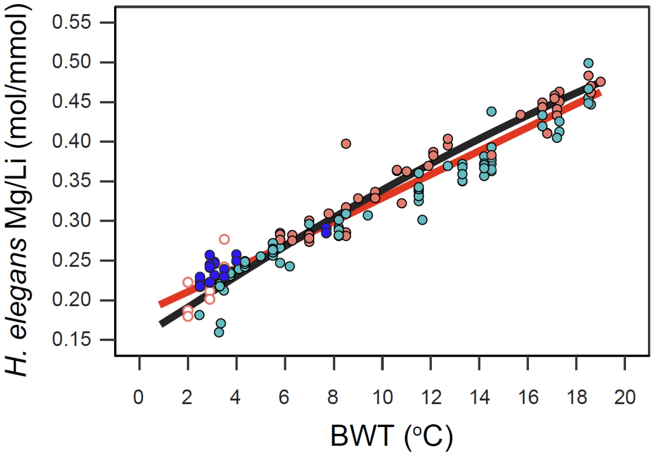
H. elegans Mg/Li (mol/mmol)
0.55
0.50
0.45
0.40
0.35
0.30
0.25
0.20
0.15
0
2
4
6
8
10
12
14
16
18
20
BWT (°C)

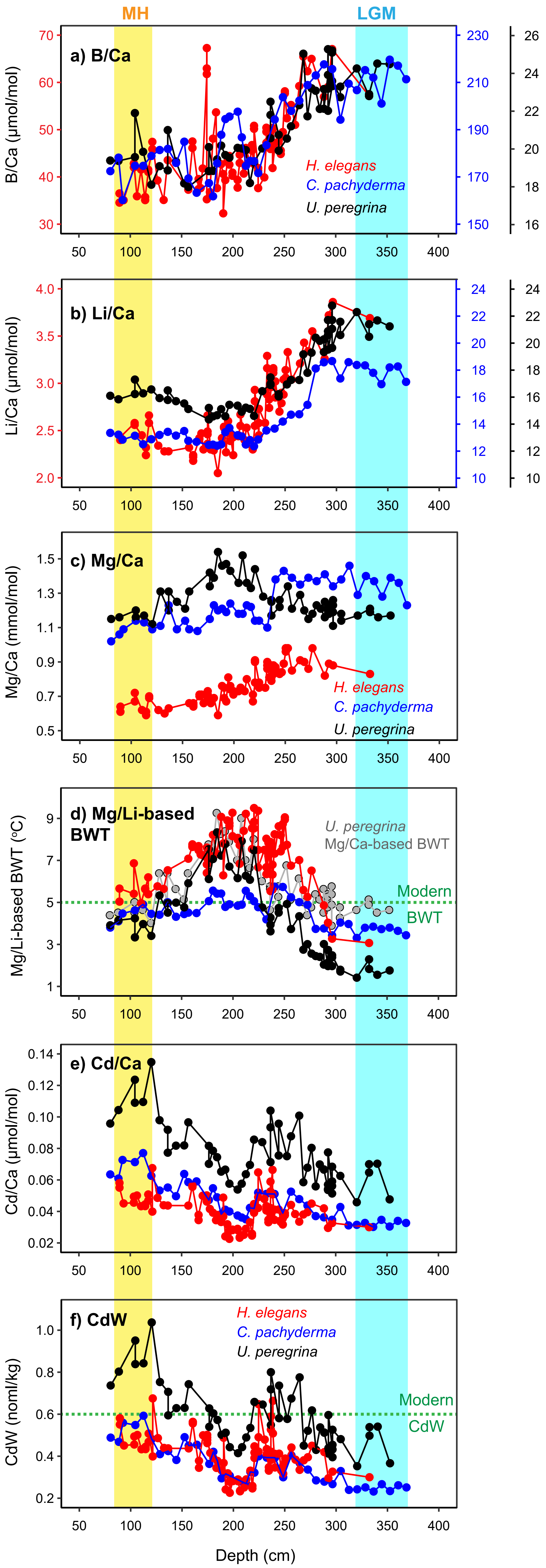
MH
LGM
a) B/Ca
B/Ca (µmol/mol)
70
60
50
40
30
230
210
190
170
150
26
24
22
20
18
16
H. elegans
C. pachyderma
U. peregrina
50
100
150
200
250
300
350
400
b) Li/Ca
Li/Ca (µmol/mol)
4.0
3.5
3.0
2.5
2.0
24
22
20
18
16
14
12
10
c) Mg/Ca
Mg/Ca (mmol/mol)
1.5
1.3
1.1
0.9
0.7
0.5
d) Mg/Li-based BWT
Mg/Li-based BWT (°C)
9
7
5
3
1
U. peregrina
Mg/Ca-based BWT
Modern
BWT
e) Cd/Ca
Cd/Ca (µmol/mol)
0.14
0.12
0.10
0.08
0.06
0.04
0.02
f) CdW
CdW (noml/kg)
1.0
0.8
0.6
0.4
0.2
Modern
CdW
Depth (cm)

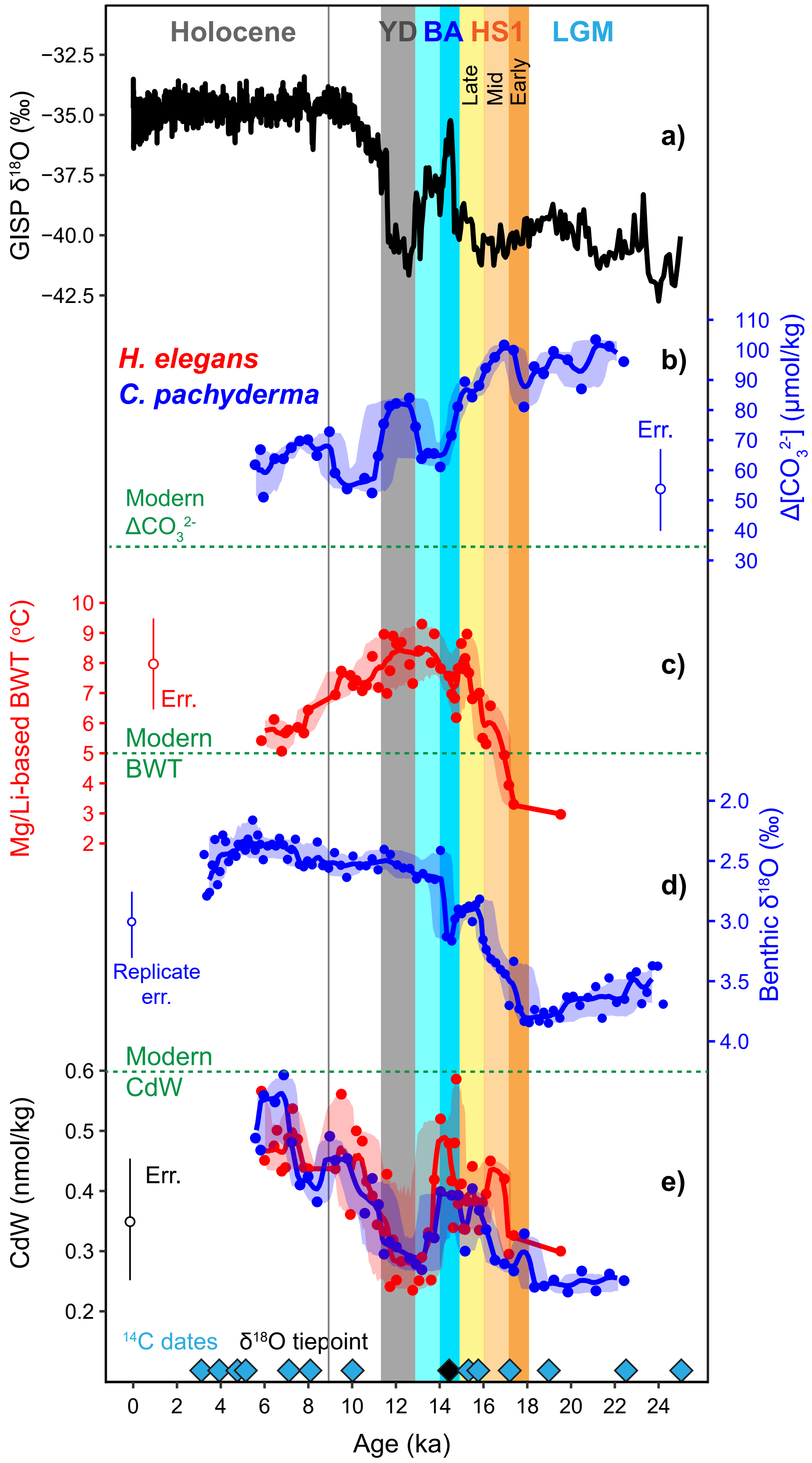
Holocene
YD
BA
HS1
LGM
Late
Mid
Early
a)
GISP δ18O (‰)
−32.5
−35.0
−37.5
−40.0
−42.5
b)
H. elegans
C. pachyderma
Err.
Modern
ΔCO3 2-
Δ[CO3 2-] (μmol/kg)
110
100
90
80
70
60
50
40
30
c)
Mg/Li-based BWT (°C)
10
9
8
7
6
5
4
3
2
Err.
Modern
BWT
d)
Benthic δ18O (‰)
2.0
2.5
3.0
3.5
4.0
Replicate
err.
e)
Modern
CdW
CdW (nmol/kg)
0.6
0.5
0.4
0.3
0.2
Err.
14C dates
δ18O tiepoint
0
2
4
6
8
10
12
14
16
18
20
22
24
Age (ka)

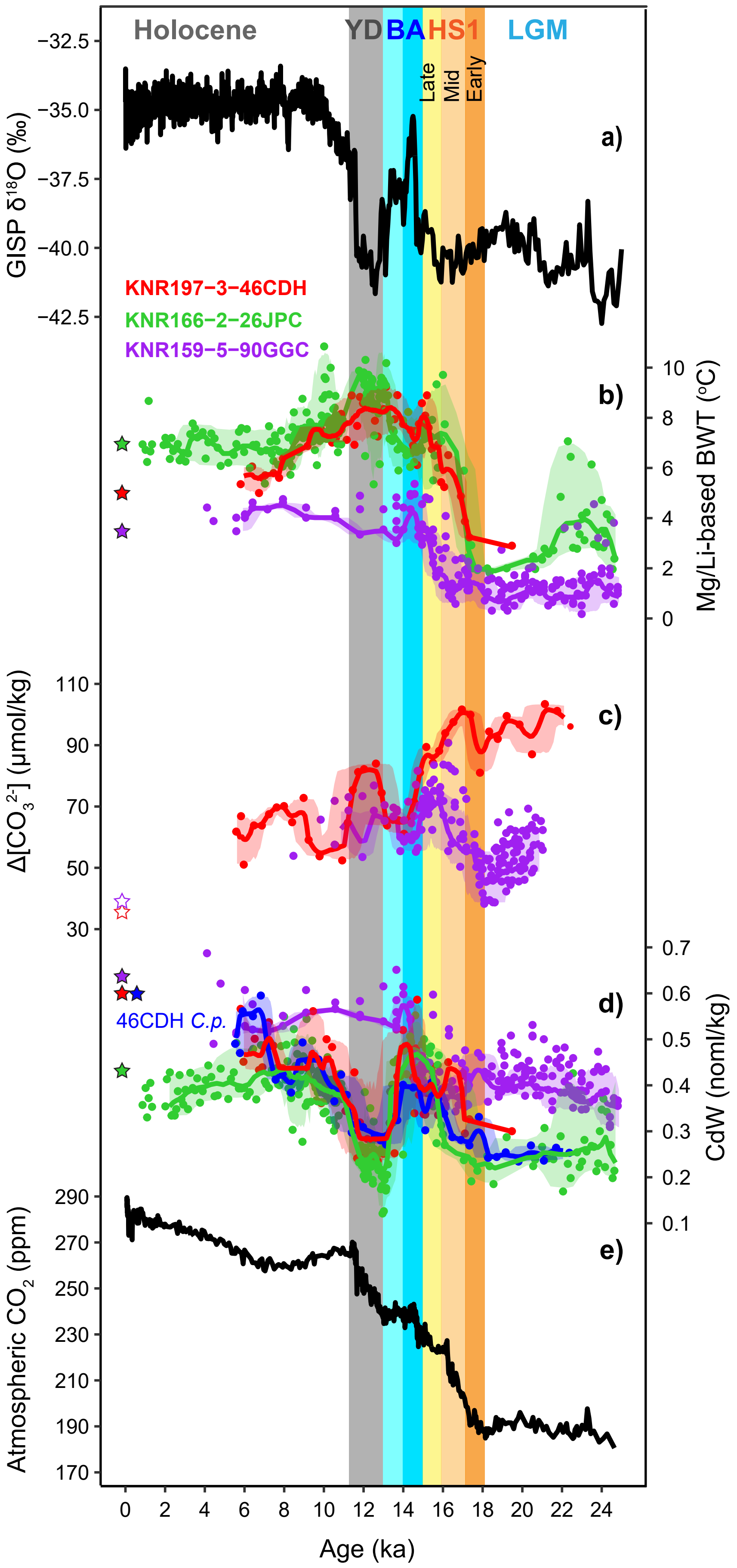
Holocene
YD
BA
HS1
LGM
Late
Mid
Early
GISP δ18O (‰)
−32.5
−35.0
−37.5
−40.0
−42.5
a)
KNR197−3−46CDH
KNR166−2−26JPC
KNR159−5−90GGC
b)
Mg/Li-based BWT (°C)
10
8
6
4
2
0
c)
Δ[CO3 2−] (μmol/kg)
110
90
70
50
30
d)
46CDH C.p.
CdW (noml/kg)
0.7
0.6
0.5
0.4
0.3
0.2
0.1
e)
Atmospheric CO2 (ppm)
290
270
250
230
210
190
170
0
2
4
6
8
10
12
14
16
18
20
22
24
Age (ka)